



RESEARCH ARTICLE

10.1029/2022JB024810

Key Points:

- A new broad-scale kinematic model has been developed spanning the 5,000 km length of the Indonesia–Australia–New Guinea collision zone
- The evolution of Cenderawasih Bay is based on the joint effect of the rotation of the Bird's Head block and the WSW drift of Weyland Thrust
- The New Guinea Fold-and-Thrust Belt experiences two transitions in its tectonic regime, as it traverses the center of the collision zone

Supporting Information:

Supporting Information may be found in the online version of this article.

Correspondence to:

S. Zhao,
Siyuan.Zhao@anu.edu.au

Citation:

Zhao, S., McClusky, S., Cummins, P. R., Miller, M. S., & Nugroho, H. (2023). New insights into crustal deformation of the Indonesia–Australia–New Guinea collision zone from a broad-scale kinematic model. *Journal of Geophysical Research: Solid Earth*, 128, e2022JB024810. <https://doi.org/10.1029/2022JB024810>

Received 19 MAY 2022

Accepted 25 JAN 2023

Author Contributions:

Conceptualization: Siyuan Zhao, Simon McClusky, Phil R. Cummins

Data curation: Siyuan Zhao, Simon McClusky, Phil R. Cummins, Meghan S. Miller, Hendro Nugroho

Formal analysis: Siyuan Zhao, Simon McClusky

Investigation: Siyuan Zhao, Phil R. Cummins

Methodology: Siyuan Zhao, Simon McClusky

New Insights Into Crustal Deformation of the Indonesia–Australia–New Guinea Collision Zone From a Broad-Scale Kinematic Model

Siyuan Zhao¹ , Simon McClusky¹ , Phil R. Cummins¹ , Meghan S. Miller¹ , and Hendro Nugroho¹ 

¹Research School of Earth Sciences, Australian National University, Canberra, ACT, Australia

Abstract The Indonesia–Australia–New Guinea collision zone comprises a complex system of tectonic blocks whose relative motion accommodates convergence of the Sunda Block, Pacific, Australian, and Philippine Sea plates. Previous studies have considered either the western or eastern ends of this system, in eastern Indonesia and Papua New Guinea, respectively. However, these studies had limited ability to characterize either the kinematics of the central part of the system or transitions in tectonic regime across it. In this study, we perform a simultaneous inversion of 492 earthquake slip vectors and 267 GPS velocities to quantify the block movement spanning the Sunda–Banda Arc, Western New Guinea, and Papua New Guinea. Our best-fitting kinematic block model comprises 23 elastic blocks, for which we estimate the rotation rates and block boundary slip rates. We show how the Cenderawasih Bay sphenochasm was likely formed by a combination of both rotations ($2.82 \pm 0.11^\circ/\text{Myr}$ anticlockwise) of the Bird's Head Block and southwest-directed convergence (39.9 ± 1.7 mm/yr) along the Lowlands fault. Our estimated relative slip vectors across the New Guinea Fold-and-Thrust Belt indicate a transition in the tectonic regime of the block boundary from predominately thrust faulting at its western segment, with a convergence rate up to 19.5 ± 0.6 mm/yr, to predominately sinistral motion in the center segment with slip rate ~ 7 mm/yr, and returning to thrust in the eastern segment with a convergence rate up to 9.0 ± 0.5 mm/yr, implying the combined effect of multiple driving mechanisms.

Plain Language Summary The Indonesia–Australia–New Guinea collision zone is an east–west elongated belt of complex tectonics at the northern edge of the Australian Plate, where the northward movement of the Australian continental lithosphere is accommodated by relative movement among a series of “microplates” in Indonesia and New Guinea. The interactions among these plates span the full gamut of tectonic phenomena. In this study, we use GPS measurements of crustal motion and earthquake data to estimate the motion of the tectonic units (plates and microplates) within the collision zone. While previous studies have considered either the western or eastern parts of this collision zone in isolation, in this study we consider together all the blocks spanning the zone from west to east. We show that this provides greater insight into changes in the tectonic regime through the center of the collision zone, and allows us to establish a new model for the development of the Cenderawasih Embayment in north-central New Guinea.

1. Introduction

We define the Indonesia–Australia–New Guinea collision zone (IANGCZ) as the area where the Australian, Philippine Sea, and Pacific Plates and the Sunda Block, all converge (Figure 1). The IANGCZ comprises the eastern islands of the Indonesian archipelago, the island of New Guinea (the Indonesian provinces of West Papua and Papua, and Papua New Guinea [PNG]), and the northern edge of continental Australia. The IANGCZ is characterized by rapid oblique convergence, resulting in complex orogenesis, frequent earthquakes, and volcanic activity (Figure 1; Figure 2; Baldwin et al., 2012; Bock et al., 2003; Hamilton et al., 1979; Koulali et al., 2015, 2016; Puntodewo et al., 1994).

Regions with active tectonic activity like the IANGCZ are often delineated in global plate models as “deforming zones” (Kreemer et al., 2014) or “orogens” (Bird, 2003), for which crustal motion data are excluded from the determination of the otherwise rigid plate motion. Even as early as the 1970s, however, it was recognized that such areas of deformation are often themselves usefully described in terms of discrete “microplates” (e.g., Alvarez et al., 1974; Dewey et al., 1973), relatively small-scale blocks with little internal deformation except near

© 2023. The Authors.

This is an open access article under the terms of the [Creative Commons Attribution License](https://creativecommons.org/licenses/by/4.0/), which permits use, distribution and reproduction in any medium, provided the original work is properly cited.

Resources: Simon McClusky, Phil R. Cummins, Meghan S. Miller, Hendro Nugroho

Software: Siyuan Zhao, Simon McClusky

Supervision: Simon McClusky, Phil R. Cummins, Meghan S. Miller

Visualization: Siyuan Zhao

Writing – original draft: Siyuan Zhao

Writing – review & editing: Siyuan Zhao, Simon McClusky, Phil R. Cummins, Meghan S. Miller, Hendro Nugroho

their edges, where much higher strains are experienced relative to the microplate interiors. While imperfect—microplate boundaries may be difficult to define, and their interiors are not perfectly rigid—kinematic microplate models have proven useful in interpreting crustal motion and earthquake data in many regions worldwide (see McCaffrey et al. (2002), for a useful overview with examples from Sumatra, Oregon, and Costa Rica). It is the approach we use in this study, building on the many previous studies that have used it to describe different parts of the IANGCZ.

Most early kinematic studies of the IANGCZ were based on earthquake and geologic data (Fitch, 1970, 1972). The first GPS measurements took place in 1991, and early studies of GPS velocities provided preliminary broad-scale estimates of relative motion between the major plates—the Australian and Pacific plates, and the Sunda Block (Puntodewo et al., 1994; Socquet et al., 2006; Stevens et al., 2002; Tregoning et al., 1994). With the ongoing development and full deployment of the GPS space segment, improvements in GPS receiver technology, and continual reductions in GPS receiver costs, more detailed GPS-based studies of microblock motions were possible. Studies in the 1990s and 2000s delineated the microblock motions of either the western part of the IANGCZ in eastern Indonesia (Bock et al., 2003; Koulali et al., 2016, 2017; Nugroho et al., 2009; Puntodewo et al., 1994; Simons et al., 2007; Socquet et al., 2006; Stevens et al., 2002; Tregoning et al., 1994), or the eastern part in Papua New Guinea (Biemiller et al., 2020; Koulali et al., 2015; Tregoning, 2002; Tregoning, Lambeck, et al., 1998; Tregoning et al., 1999, 2000; Wallace et al., 2004, 2014). However, as indicated in Figure 1, several major faults extend from the western to the eastern part of the IANGCZ, and these are likely associated with large-scale deformation affecting both regions. Without considering the full breadth of the IANGCZ, previous kinematic models cannot fully and accurately characterize changes in tectonic regimes along such faults.

In addition, in the central part of the IANGCZ—the Indonesian provinces of Papua and West Papua, as well as western PNG—the kinematic studies are fewer and mainly focus on the Bird's Head region or regard all of Western New Guinea as a single block, due to the lack of data and the remoteness of the region (e.g., Bock et al., 2003; Pubellier & Ego, 2002; Stevens et al., 2002). The paucity of GPS data to constrain detailed kinematic models in the Banda Sea and West New Guinea led to a wide-ranging debate on the origin and mechanism of the tectonic structures in this area. For example, the tectonic evolution of Cenderawasih Bay (Babault et al., 2018; Charlton, 2000, 2010; François et al., 2016); along-strike changes in motion along the New Guinea Fold-and-Thrust Belt (NGFTB (Baldwin et al., 2012; Cloos, 2005; Hill et al., 2003);) and the driving mechanism of some highly active faults (like the Tarera-Adiuna fault, Lengguru fault, and Seram Trough; Bailly et al., 2009; Baldwin et al., 2012; Cloos, 2005). These studies are mainly based on geological and seismic data, and the deformation in this complex plate boundary zone has not been well quantified. Due to the lack of GPS measurements, it is difficult to determine the micro-block boundaries of a more sophisticated model. Therefore, the previous kinematic results for West New Guinea have significant uncertainties, and the motion rates for the deformation area have not all been accurately estimated.

To address the issues mentioned above, we develop a broad-scale kinematic model that spans 5,000 km from longitude 110°E to 156°E, which in addition to microblocks in the western and eastern IANGCZ taken from the studies mentioned above, includes several new microplates in western New Guinea, as described below. For western New Guinea, the reprocessed data from 28 GPS sites allow us to develop a completely new model that includes the Bird's Head Block and six new microplates in the central portion of the IANGCZ. These are the Yapen, Cendrawasih Bay, Tarera-Adiuna, Forearc, and West New Guinea Highland blocks, and the Mamberamo deformation zone (YAPE, CEND, TABL, FORE, WNGH, and MDZ, respectively; Figure 3a). Also, some block boundaries defined in previous studies are adjusted to optimize the fit to the full dataset. Our new model links up the broader kinematic picture between PNG, Western New Guinea, and east Indonesia, which emphasizes first-order kinematic characteristics associated with deformation along the large-scale tectonic structures. We synthesize the previous regional GPS studies in conjunction with newly available geologic and seismologic observations from across the region to develop a consistent and coherent kinematic description for the whole IANGCZ.

2. Tectonic Setting and Kinematic Blocks

The east-west trending IANGCZ accommodates relative plate motion between the major tectonic plates through a complex system of fault-bounded tectonic blocks (Socquet et al., 2006; Stevens et al., 2002; Tregoning et al., 2000; Wallace et al., 2004). In this section, we consider the details of the tectonic setting along the IANGCZ, starting

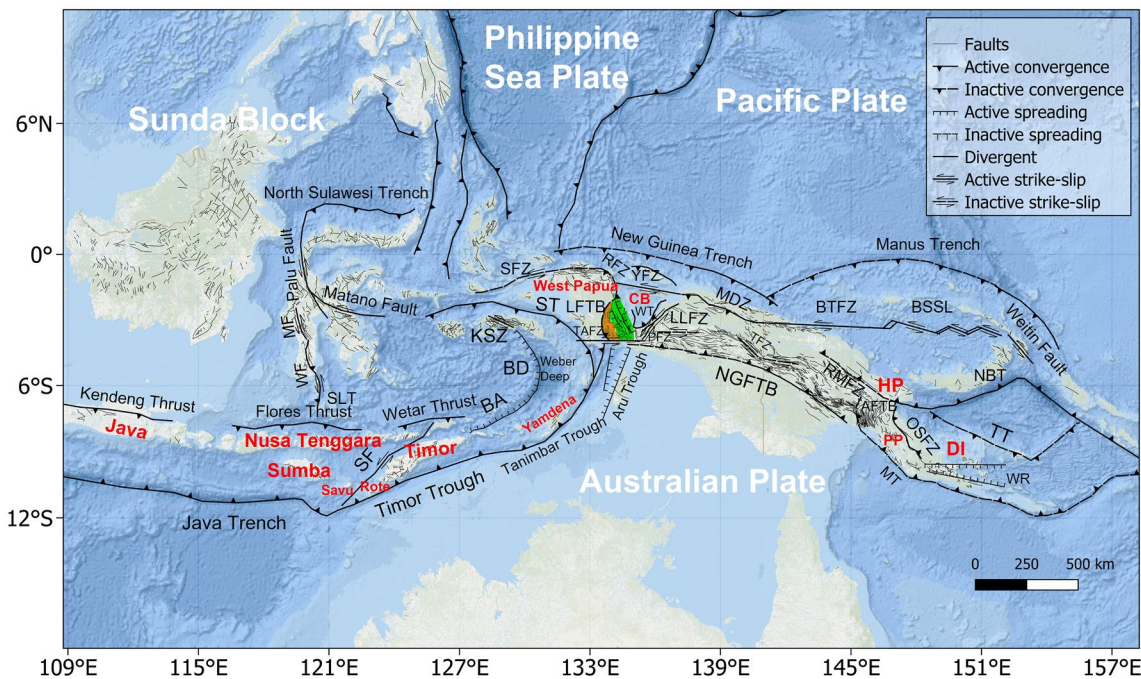


Figure 1. Topography and tectonic map of Indonesia–Australia–New Guinea collision zone. Tectonic boundaries are derived from Baldwin et al. (2012), Chen et al. (2019), Cloos (2005), Cummins et al. (2020), François et al. (2016), Jaya and Nishikawa (2013), Koulali et al. (2015), and Spencer et al. (2016). Faults are from the East and Southeast Asia (CCOP) 1:2,000,000 geological map (downloaded from <https://www.orrbodies.com/resource/ccop-geology-south-east-asia/>). AFTB: Aure Fold-and-Thrust Belt; BSSL: Bismarck Sea seismic lineation; BTFZ: Bewani-Torricelli fault zone; BA: Banda Arc; BD: Banda Detachment; CB: Cenderawasih Bay; DI: D’Entrecasteaux Islands; HP: Huon peninsula; KSZ: Kawa Shear Zone; LFTB: Lengguru Fold-and-Thrust Belt; LFZ: Lagaip fault zone; LLFZ: Lowlands Fault; NBT: New Britain Trench; MDZ: Mamberamo deformation zone; MF: Masupu Fault; MT: Moresby Trough; NGFTB: New Guinea Fold-and-Thrust Belt; OSFZ: Owen Stanley fault zone; PFZ: Paniai fault zone; PP: Papuan peninsula; PTFB: Papuan thrust-and-fold belt; RFZ: Ransiki fault zone; RMFZ: Ramu-Markham fault zone; SF: Semau Fault; SFZ: Sorong fault zone; SLT: Selayar Thrust; ST: Seram Trench; TAFZ: Tarera-Aiduna fault zone; TFZ: Tahin fault zone; TT: Trobriand Trough; WR: Woodlark Rift; WF: Walanae Fault; WT: Weyland Thrust; YFZ: Yapen fault zone. The green patch represents the external zone of the Lengguru fault, showing different tectonic regimes.

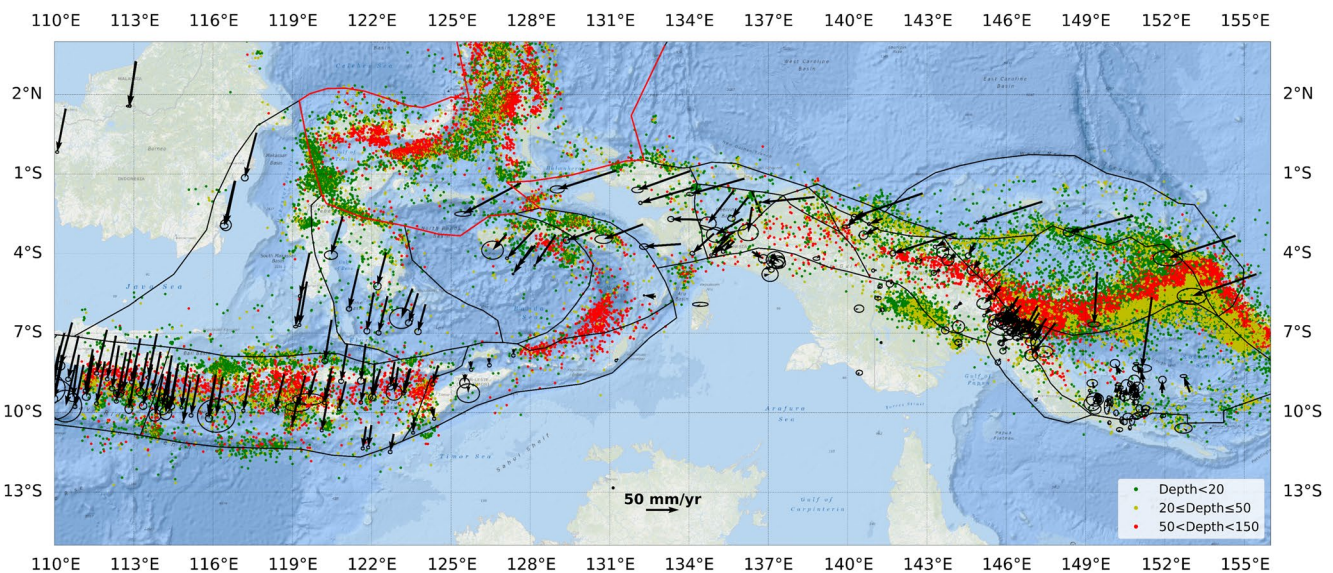


Figure 2. The global positioning system (GPS) velocity field with 95% confidence interval ellipses was utilized in this study with respect to the Australian Plate. The names of the GPS sites are shown in Table S1 of Supporting Information S1. In the Sunda-Banda region and West New Guinea, the relocated seismicity data ($M_w \geq 5$) are derived from Supendi et al. (2020), from 2009 to 2018, with depth of less than 150 km. In the Papua New Guinea area, the relocated seismicity data ($M_w \geq 5$) are derived from the ISC Bulletin catalog with the same time and depth range. The solid red lines represent the free-slipping boundaries (locking constrained to zero); the solid black lines represent the block boundaries.

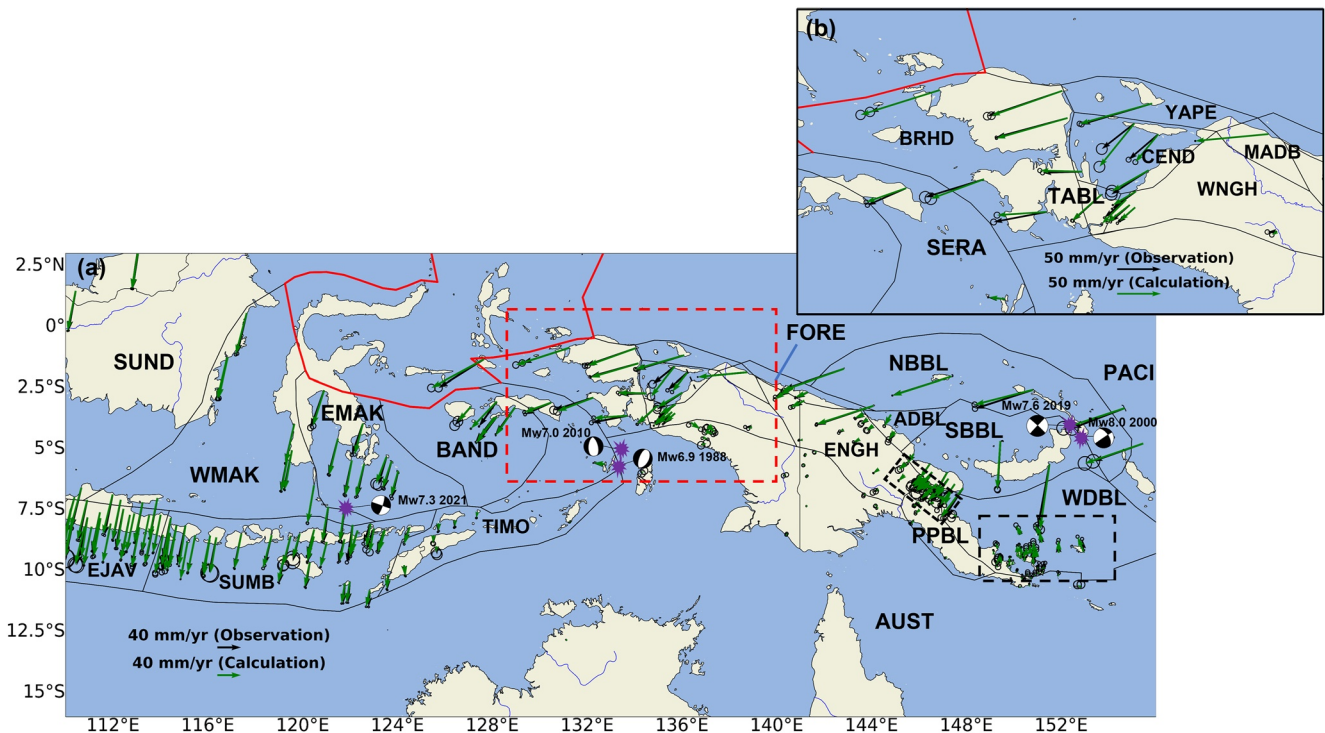


Figure 3. (a) Map showing our best-fit block model consisting of 23 plates/blocks. Abbreviations are Sunda block (SUND), East Java block (EJAV), Sumba block (SUMB), West Makassar block (WMAK), East Makassar block (EMAK), Timor block (TIMO), Banda block (BAND), Seram block (SERA), Bird's Head block (BRHD), Yapen block (YAPE), Cendrawasih Bay block (CEND), Tarera-Adiuna fault zone block (TABL), Mamberamo deformation zone block (MADB), Forearc block (FORE), West New Guinea Highland block (WNGH), East New Guinea Highland block (ENGH), North Bismarck block (NBBL), South Bismarck block (SBBL), Adelbert block (ADBL), Papuan Peninsula block (PPBL), Woodlark block (WDBL), Australian Plate (AUST), and Pacific Plate (PACI). The focal mechanisms are derived from GCMT. (b) The inset figure corresponds to the red dashed rectangle area in panel a, showing the close-up view of the observed and modeled global positioning system velocities in Western New Guinea. The zoomed-in view of the two black dashed rectangle areas (Ramu-Markham fault zone and Woodlark Rise) are shown in Figure S4a and Figure S4b of Supporting Information S1, respectively.

from eastern Java in the west and proceeding eastward to Papua New Guinea. We refer to Figure 1 for the locations of faults, deformation zones, fold-and-thrust belts, etc., and Figure 3 for the names of the blocks/microplates.

The western part of the IANGCZ has a tectonic setting that continuously transitions from subduction of Australian plate oceanic lithosphere south of Java to arc-continent collision in the Lesser Sunda Islands, in the western part of the Banda Arc. The Australian Plate has migrated northward rapidly since the Eocene, leading to the subduction beneath Java (Hall, 2011). This northward movement is also associated with the collision of the Australian continental lithosphere with the western Banda arc that began in the Pliocene (Hall, 2011; Roosmawati & Harris, 2009). This region marks a transition from Eurasian tectonic units in Java and Bali to Australian units in the Sumba and Savu Islands (Harris et al., 2009). Fold-and-thrust structures have been inferred from marine seismic surveys and the seismicity distribution, suggesting that back-arc thrusting occurs off the northern shores of Flores and Sumbawa Islands (McCaffrey & Nábělek, 1984; Silver et al., 1983). This back-arc thrust system, referred to as the Flores Back-arc Thrust (FBT), seems likely to have an important bearing on the evolution of the convergent margin.

Global Positioning System (GPS) measurements of crustal deformation in this region demonstrate how the convergence between the Australian and Sunda Plate transitions from 95% accommodation at the subduction megathrust off eastern Java to 40% accommodation taking place along the FBT; this is in addition to strike-slip motion along the Semau Fault, stretching from the western tip of Timor to the island of Alor (Koulali et al., 2016; Nugroho et al., 2009). This variation in convergence style between eastern Java and the Banda Arc is associated with the lateral offset of continental collision and oceanic subduction (Miller et al., 2021). In one of the most recent GPS studies of eastern Indonesia, Koulali et al. (2016) divided the Sunda-Banda Arc into the three microblocks: East Java, Sumba, and Timor (EJAV, SUMB, and TIMO, respectively, in Figure 3). Taking six new GPS velocities located in the Banda area into account, Cummins et al. (2020) revised the block geometry

of Koulali et al. (2016) by using the active Banda detachment fault as a block boundary that separates the Banda block of Koulali et al. (2016) into the two microblocks, Banda and Seram (BAND and SERA in Figure 3a).

The Banda arc in the central part of the IANGCZ is well known for its near 180° bend within a tight 350 km radius of curvature. However, the formation of this spectacular curve has long been the subject of debate; there are two main hypotheses, the single-slab model and the two-slab model (Baldwin et al., 2012; Carter et al., 1976; Hamilton et al., 1979; Hinschberger et al., 2000, 2001; Spakman & Hall, 2010). According to the model of Chase (1978), based on intraslab seismicity, two plates are subducting beneath the Banda Sea. One subducts from the north at the Seram Trough, and the other subducts from the south at the Aru and Timor troughs. Where the Seram and Aru Troughs merge at the eastern end of the Banda Arc, they are separated by the sinistral Tarera–Aiduna Fault (Figure 1). These results were reinforced by later studies mainly based on fault plane solutions of earthquakes in Western New Guinea and the Banda arc (Abers, 1989; Das, 2004). However, Spakman and Hall (2010) put forward a single-slab model which indicates that the spoon-shaped structure of the Banda slab is primarily caused by the rollback of dense oceanic lithosphere into an embayment enclosed by the continental crust of the Australian plate. This hypothesis also explains the lack of oceanic lithosphere, or signs of its consumption, between the Seram and Bird's Head blocks. It is further hypothesized that this slab rollback has driven lithospheric extension in the Banda Sea, much of which is accommodated by a massive normal fault known as the Banda Detachment on the western margin of the Weber Deep (Pownall et al., 2016).

East of the Banda Arc, the outline of the island of New Guinea is often described as having the shape of a bird, and it is divided geographically from west to east into the Bird's Head, Neck, Body, and Tail segments, as described in many studies (e.g., Cloos, 2005). The Seram Trough, Sorong Fault, and Lengguru fold-and-thrust belt make up the Bird's Head region, which converges obliquely with Seram Island at the Seram Trough, driving a sinistral shear zone (Bock et al., 2003; Pubellier & Ego, 2002; Stevens et al., 2002). The Lengguru fault zone consists of internal and external zones, which have different tectonic regimes (Bailly et al., 2009). The internal zone is undergoing active extension which is believed to have started ~3 Ma, whilst the external zone is a compressional regime that accommodates the Australia-Pacific collision. The nature of this young extensional structure is still under debate (Babault et al., 2018; Bailly et al., 2009; Charlton, 2000). The Tarera–Aiduna fault zone is the southern boundary of the Bird's Head and Neck regions, comprising a set of highly active east-west trending sinistral echelon faults (Hamilton et al., 1979; Katili, 1986; McCaffrey, 1989; Watkinson & Hall, 2017). For most of its length, the Tarera–Aiduna Fault strikes almost parallel to the western end of the New Guinea Fold-Thrust Belt to the south, before it is terminated in an asymmetrical graben consisting of several NE–SW trending normal faults (Watkinson & Hall, 2017). Hence, the eastern Tarera–Aiduna Fault is highly seismically active with different stress regimes.

Cenderawasih Bay is a north-opening triangular embayment linking the Bird's Head block to the Central Ranges (Bird's Body) of mainland New Guinea (Babault et al., 2018). Charlton (2000), and Charlton (2010) described the Cendrawasih Bay region as a triangular embayment formed by the 30~40° anticlockwise rotation of the Bird's Head block with respect to the Australian Plate since ~5 Mya, which suggests a rotation rate of 6~8°/Myr. However, according to some stratigraphic and geomorphologic studies (e.g., Babault et al., 2018; Dow & Sukanto, 1984; François et al., 2016), the geometry of Cenderawasih Bay has not changed significantly since the Neogene collision. François et al. (2016) suggested that the Bird's Head block and the Lengguru Fold-and-Thrust Belt both belonged to the north Australian passive margin before the Neogene collision, and their southwestward drift in the late Miocene resulted in the formation of Cenderawasih Bay, a hypothesis that was supported by Babault et al. (2018) by combining drainage network analysis, interpretation of seismic lines and thermochronological data assessment.

The GPS measurements from 1991 to 1997 show 75.0 to 80.0 mm/yr southwest motion of Bird's Head block (BRHD, Figure 3) relative to Australia along a wide shear zone (Stevens et al., 2002). This result is consistent with the study of Pubellier and Ego (2002), which suggested that the BRHD of West New Papua is an example of escape tectonics, resulting from the collision between the remnants of volcanic belts carried by the Pacific Plate and the Australian Plate with the rate reaching 70.0 mm/yr based on seismicity, micro-tectonic data, and synthetic aperture radar. Bock et al. (2003) generated a relatively simple kinematic model for Western New Guinea, which regarded the Bird's Head region and Cenderawasih Bay as a single block. They computed the Euler pole of rotation for the Bird's Head block, suggesting that it rotated anticlockwise at the rate of $2.92 \pm 0.45^\circ/\text{Myr}$ with respect to the Australian Plate.

There are two active inland deformation areas in the Bird's Body section, the Memberamo deformation zone and the New Guinea Fold and Thrust Belt (NGFTB). The Memberamo region is characterized by fields of active mud volcanoes and an irregular swampy landscape. It has been regarded as a broad compressive arc that connects the Yapen and Bewani-Torricelli sinistral strike-slip fault zones (Sapiie et al., 1999; Williams et al., 1984). Further west, the Yapen fault links with the Sorong fault zone (Baldwin et al., 2012).

The NGFTB is a 4-km-high, 1,300-km-long, E-W trending mountain belt, which stretches from the Bird's Neck (at the eastern Tarera-Aiduna Fault) to its Tail (west of the Papuan Peninsula) (Abers, 1989; Baldwin et al., 2012; Bock et al., 2003; Cloos, 2005). Convergence resulting from the oblique collision between the Australian Plate and the Pacific Plate is partially accommodated by sinistral motion on the Tarera–Aiduna Fault in western New Guinea and reactivation of the thrust front of the NGFTB (Abers & McCaffrey, 1988; Dow & Sukanto, 1984; Puntodewo et al., 1994). The convergence rate between the Australian and Pacific plates is around 110 mm/yr, and only 5%–20% of the convergence is accommodated by the NGFTB based on the volume of the uplifted mountain range and present-day earthquake activity (Abers & McCaffrey, 1988; Bock et al., 2003). The other candidates for the accommodation of the remaining convergence are the New Guinea Trench inside the Bird's Body section, and a complicated array of microplates with a variety of plate boundary types in the Bird's Tail region, including a strike-slip transform system (Bismarck Sea Seismic Lineation [BSSL]; Taylor, 1979), collision orogenesis (Abers & McCaffrey, 1988, 1994; Finisterre Arc; Silver et al., 1991), a rifting system (Woodlark; Taylor et al., 1991) and subduction zones (New Britain Trench; Silver et al., 1991).

The active Bismarck Sea Seismic Lineation (BSSL) is a zone of spreading segments and sinistral transform faults which separates the Bismarck Sea into South Bismarck (SBBL) and North Bismarck (NBBL) blocks (Taylor et al., 1991; Tregoning et al., 1999). The subduction of the Solomon Sea forms the New Britain Trench (NBT), which also drives the seafloor spreading and rifting in the Woodlark Basin and Woodlark Rift (WR), respectively (Weissel et al., 1982). The style of the plate boundary between the Australian and Woodlark plate accommodates a transition from divergence (the Woodlark Rift) to convergence (the Papuan Peninsula) over 500 km, along a reactivated megathrust known as the Owen-Stanley fault zone, which connects with the Ramu-Markham fault that is formed due to the collision between the New Guinea Highland Block and the SBS block (Davies & Smith, 1971; Ott & Mann, 2015; Wallace et al., 2004).

In PNG, the first tectonic block model was developed by Tregoning, Lambeck, et al. (1998), which divided the PNG area into South Bismarck and Woodlark blocks (SBBL and WDBL, Figure 3a). Tregoning (2002) added a new block (North Bismarck block denoted NBBL in Figure 3a) into their PNG model. The Eastern New Guinea Highland, Adelbert, and Papuan Peninsula blocks (ENGH, ADBL, and PPBL) were proposed and analyzed by Wallace et al. (2004, 2014). Wallace et al. (2004) used GPS data in the New Guinea Highlands to show the ENGH has motion distinct from the Australian Plate, and similarly proposed the existence of a separate ADBL. They simultaneously estimated block Euler vectors in eastern New Guinea and interseismic fault locking on the Ramu Markham Fault using a densified network of sites through the New Guinea Highlands and Finisterre collision zone, adding 35 new sites to the previously sparse network in the region. In contrast, the model of Koulali et al. (2015) included additional data from the New Guinea Highlands region and found that the ENGH rotates clockwise about a pole located northwest of the block. Wallace et al. (2014) made geodetic measurements at a dense network of sites in the Woodlark Basin/Papuan Peninsula region in southeast Papua New Guinea, to undertake a detailed assessment of the distribution and rates of rifting in the WR, defining several microblocks along the WR.

3. Data and Method

3.1. GPS Velocities and Earthquake Slip Vectors

We reprocessed GPS observations collected from 28 campaign stations located in West New Guinea and acquired two new GPS data from the stations at Timor Island (McCaffrey, 2002, 2005). The reprocessed data were collected from 2002 to 2004 and processed using the GAMIT/Global Kalman Filter (GLOBK) software suite (Herring et al., 2010; Herring, King, & McCusky, 2015; Herring, King, Flyod & McClusky, 2015). The GPS sites were observed with three different antenna and receiver combinations: TRM29659.00/Trimble 4000 SSI, TRM41249.00/Trimble 5700, and ASH701975.01A-GP/Ashtech UZ-12.

In East Timor, new GPS observations from the stations DILI and SAME were processed. The DILI station is a semi-permanent station occupied from 2018 to 2019. The SAME station is a campaign station that has been

surveyed in 2005, 2018, and 2019. Both stations were occupied using TRM39105.00/Trimble 5700. The GPS data processing procedure follows the two-step approach described by Reilinger et al. (2006). In the first stage, we used GAMIT to obtain the 'h-files', a loosely constrained covariance matrix of station positions. Using GAMIT, the ionosphere-free combination of phase observations was used to estimate station positions, phase ambiguities, earth rotation parameters, and the zenith troposphere delay while the International GNSS Service (IGS) final satellite orbits were held fixed. The IERS2010 standard solid Earth tide and sub-daily earth rotation correction models and the FES2004 ocean tide loading model corrections computed by the Onsala Space Observatory were applied. In the second stage, we used the GLOBK to combine data in a single solution and generate velocity field estimates and position time-series. We include the GPS data from 13 continuous IGS global stations to tie our local network into the ITRF 2014 reference frame. We also used the first-order Gauss–Markov extrapolation algorithm described in Herring, King, and McClusky (2015) to estimate the realistic noise properties of the GPS time-series used to scale the estimates of velocity uncertainties. This procedure has been used previously and reviewed extensively in many studies (e.g., Koulali et al., 2015, 2016, 2017; Reilinger et al., 2006; Wallace et al., 2004, 2014). The position time-series are examined for offsets and outliers, resulting from antenna changes or earthquakes (Tregoning et al., 2013). However, the GPS sites at Western New Guinea are not temporally dense enough to enable correcting of the coseismic offsets. Therefore, we excluded the nine GPS velocities which were displaced coseismically by a series of earthquakes with $M_w \geq 5.5$ that occurred at the southern Lowland faults and northern Lengguru fault, between 2002 and 2004 in Western New Guinea (Figure S1 of Supporting Information S1).

We combined the velocity estimates from the 28 reprocessed and two newly processed stations with the velocities published in previous studies, including Biemiller et al. (2020); Bock et al. (2003); Cummins et al. (2020); Genrich et al. (1996), Koulali et al. (2015, 2016, 2017); Kreemer et al. (2014); Meilano et al. (2021); Phillips (2003); Tregoning, Lambeck, et al. (1998); Tregoning, Tan, et al. (1998); Tregoning et al. (1999); Stevens et al. (2002); Simons et al. (2007); Wallace et al. (2004, 2014). Since this study combined data from several different solutions and studies, there are often multiple velocity estimates available for sites; in this case, we computed the weighted average of the velocity estimates which are within two standard deviations, and we also considered the uncertainty of the estimates from different studies. After removing duplicates and outliers as described above, 267 high-quality GPS velocities were selected for inversion. Finally, in order to better analyze the kinematic pattern of the entire broad-scale model, we choose the Australia Plate which interacts with the entire length of the IANGCZ as the reference frame. All the velocity solutions were optimally rotated into the Australia-fixed reference frame by resolving a rotation of the dataset that minimizes the velocities at the sites located in the Australia Plate using TDEFNODE (McCaffrey, 2009), which applies simulated annealing to downhill simplex minimization (Press et al., 1989). The 267 GPS velocities are presented and plotted in an Australian-fixed reference frame in Table S1 of Supporting Information S1, Dataset S1 of Supporting Information S1, Figure 2, and Figure S2 of Supporting Information S1.

Earthquake slip vectors are derived from earthquake focal mechanisms, which provide important information about the directions of plate motion in estimating the Eulerian pole of each block/plate (Aki & Richards, 1980; DeMets et al., 1990, 1994). For the kinematic modeling, earthquake slip vectors can be used to constrain the azimuth of block motions (Koulali et al., 2015, 2016; Tregoning & McQueen, 2001; Wallace et al., 2004). In our study, we utilized 492 earthquake slip vector azimuths in total (Figure S3 of Supporting Information S1; Dataset S2 of Supporting Information S1). Most of them are derived from the Global Centroid Moment Tensor (GCMT; Ekström et al., 2012) catalog for events shallower than 100 km and $M_w > 5.5$ from 1976 to 2018. We also include the earthquake slip vectors used in Koulali et al. (2015). We allowed 20° uncertainties in slip orientation in the inversion. Since for any moment tensor, there are two nodal planes, either of which may correspond to the actual fault plane, each calculated earthquake slip vector can have one of two possible azimuths (Cronin, 2004). Hence, we made geologically reasonable choices for the slip vectors, by considering the detailed tectonic maps and mapped faults (Figure 1).

3.2. Kinematic Modeling

Observed long-term crustal velocities can be modeled as a sum of high rates of internal strain accumulation in the areas adjacent to block boundaries and rigid block rotations specified by Euler pole rotations (McCaffrey et al., 2000, 2002; Meade & Hager, 2005). We follow the block modeling method in TDEFNODE (McCaffrey, 2009), which specifies the block motions via angular velocities on the surface of a sphere and

applies interseismic “back-slip” along the block boundaries (Savage & Burford, 1973). All the GPS velocities and earthquake slip vectors are inverted simultaneously to estimate the Euler vectors of blocks and coupling fractions, defined as the ratio of locked to total slip on the major block boundary faults. Block boundaries are the most important prerequisites for the inversion, and they were initially determined from the seismicity ($M_w \geq 5$) distribution (Figure 2), GPS velocity field (Figure 2), mapped faults (Figure 1), and the models from previous studies (e.g., Bock et al., 2003; Cummins et al., 2020; Koulali et al., 2015, 2016; Stevens et al., 2002; Wallace et al., 2004, 2014). The choice of threshold magnitude for earthquake data varies among the previous kinematic studies, which choose a similar or even smaller magnitude threshold than used here for the initial boundary determination (Koulali et al., 2015, 2016; Reilinger et al., 2006; Wallace et al., 2004, 2014). The block boundaries were then adjusted by minimizing the data misfit as expressed by the chi-square statistic χ_n^2 value and applying the ratio F -test to verify the significance of fit improvement (Stein & Gordon, 1984).

In Western New Guinea, the downdip geometry for the subduction zone is based on the U.S Geological Survey's Slab 2.0 model (Hayes, 2018), and seismicity cross-sections for the other block boundary faults not covered by Slab 2.0 (e.g., Lengguru fault zone, Lowlands fault zone, Ransiki fault zone, and Mamberamo deformation zone). Fault nodes are placed along the depth contours of the faults, every 5 km in the upper 30 km and every 10 km from 30 to 50 km. We considered as free-slip (i.e., locking is constrained to zero) boundaries those block boundaries that are less well determined due to: the lack of historical earthquakes; no coverage by the Slab 2.0 model; lack of good GPS coverage and/or ambiguity in the tectonic maps (Figure 1). As described above, in the Sunda-Banda region and PNG, most boundary faults and block geometries are mainly described based on Koulali et al. (2015, 2016), respectively. Compared to Koulali et al. (2015), Wallace et al. (2014) have given the Woodlark region, southeast PNG, a more detailed kinematic analysis, including additional microblocks. Considering that the main aim of our study is to investigate the large-scale first-order tectonic structures, our southeast PNG block geometries were derived from the simpler model in Koulali et al. (2015), rather than attempting to reproduce the work in Wallace et al. (2014). However, some geometries of the blocks located in the central IANGCZ (e.g., FORE and ENGH blocks) are revised in this study according to recently mapped faults, updated GPS velocity field, and relocated seismicity distribution so that the merged broad-scale block model is tectonically and geodetically reasonable. The updated GPS velocities give us more comprehensive observations of the deformation, which allows us to improve the block model constraints. We parameterize the locking along the Sunda-Banda forearc and Flores back-arc thrust as a modified Wang et al. (2003) function such that the full coupling ratio ($\Phi = 1$) decreases down-dip exponentially until no coupling ($\Phi = 0$). The depth of the top and bottom of the transition zone are parameters determined by the inversion. The locking parameters for the active boundaries of PPBL, SBBL, NBBL, and WDBL are derived from the previous PNG kinematic model in Koulali et al. (2015). The parameterization of the other boundary faults in our model is simplified by fixing uniform locking to the depth of 10~20 km, in order to reduce the number of free parameters.

4. Preferred Best-Fit Model Geometries

Our best-fit kinematic model consists of 23 crustal blocks (Figure 3) and was compared with 10 models having different geometrical configurations (Figure S5 and Table S3 of Supporting Information S1). We compare the values of normalized root mean square (NRMS) and weight root mean square (WRMS) of the corresponding blocks in the different models, which provides a statistical measurement of the variance between the predicted values and observed GPS velocity values on common blocks (Barondess & Utku, 1963; Chen et al., 2010; Di Piazza et al., 2016; Willmott & Matsuura, 2006). The F -ratio test put forward by Stein and Gordon (1984) is also performed in this study to verify the significance of changes in the fit between competing models (Table S3 of Supporting Information S1). The best-fit model suggests a higher goodness-of-fit for the earthquake slip vectors in the eastern PNG area (Figure S3 of Supporting Information S1). This is consistent with the deformation in the Bismarck Sea seismic lineation and NBT in eastern PNG being predominantly controlled by the high-slip first-order tectonic structures. Whereas some deformation zones in the Banda arc and West New Guinea regions (e.g., Lowlands and Lengguru fault zones) comprise a series of small-scale faults with similar regimes, which leads to the relatively high residuals, as our model simplifies these deformation zones as single large-scale tectonic boundaries.

In Western New Guinea, we suggest a new model geometry that subdivides the region into eight micro-blocks. Unlike previous studies (e.g., Bock et al., 2003; Stevens et al., 2002), which defined the Bird's Head and Neck

regions as a single block, we consider the Bird's Head and Neck regions as separate blocks. We split the Cenderawasih Bay area into three micro-blocks (YAPE, CEND, and TABL) using the Biak Thrust, Yapen Fault, Weyland Overthrust, Lowlands fault zone, Lengguru fold-and-thrust belt, and Tarera-Adiuna Fault as the active block boundaries. The highly seismically active MDZ connects sinistral strike-slip motion on the Yapen Fault in the west with the same style motion on the Bewani-Torricelli fault in the east (Cloos, 2005; Sapiie et al., 1999). Together these are considered as the southern boundary of the FORE block in our study. According to the distribution of the historic earthquakes in this area (Figure 2), the southeast tip of the MDZ connects with the sinistral Tahin fault zone (Figure 1), which separates the Bird's Body region into WNGH and ENGH blocks (Figure 3). Although the seismological data illustrates that the WNGH and CEND blocks could be subdivided into more complex configurations, additional microblocks will not improve the goodness of fit statistically due to the low density of GPS observations (Figure 3).

For the Sunda-Banda area, we applied similar block geometries to Koulali et al. (2016). However, since new GPS observations from the Banda region were used in the inversion, the previous kinematic model configurations from Koulali et al. (2016) illustrated distinct residuals, especially for site CUAL, which revealed that the Tual Island site should not be modeled in the TIMO block (Figure S5b of Supporting Information S1). Cummins et al. (2020) put Tual Island (site CUAL) and Yamdena Island (site CSAU) into the same SERA block, obtaining a relatively small residual at each site, whilst the SERA block exhibited large NRMS/WRMS and χ_n^2 values (9.14/2.69 and 11.1, respectively), (Figure S5c of Supporting Information S1). We found that these NRMS/WRMS and χ_n^2 values for the SERA block can significantly decrease to 2.71/0.75 and 9.4 when the site CSAU is instead included in the TIMO block, while for the TIMO block, the statistic measurements did not show a demonstrable change. This indicates that the tectonic block in which site CSAU is located has the same kinematic properties as the sites in the TIMO block. Hence, we modeled the SERA block as one curved block, including the entire Weber deep and bounded in the east by the Aru and Seram Troughs, and bounded in the west by the Banda Detachment and Kawa Shear Zone, which cuts through the length of Seram Island. We merge Yamdena Island into the TIMO block, utilizing the Timor Trough and Tanimbar Trough as the southern boundary of the TIMO block. We utilized a boundary based on seismicity separating the TIMO and SERA blocks to decrease the χ_n^2 value and satisfy an *F*-test (Figure S5 and Table S3 of Supporting Information S1). This new boundary setting is consistent with the seismic zone defined by Rahmadani et al. (2022).

Koulali et al. (2016) defined the boundary between the Western and Eastern Makassar Blocks (WMAK and EMAK, respectively) by combining the southern Palu, Masupu, and Walanae Faults, extending the latter offshore along the Selayar Trough, and then continuing this boundary in a southward direction until it connects with the Flores Back-arc Thrust. We note, however, that this latter southward extension is not well supported by bathymetry or seismicity, and does not follow the Selayar Islands chain where it bends sharply eastward, just south of the Selayar Trough. In December 2021 a large, Mw 7.3 earthquake occurred with a dextral rupture along a fault oriented along this southeast extension of the Selayar Islands chain (GCMT). We have therefore adjusted the EMAK/EMAK boundary to follow this eastward bend in the Selayar island chain, extending southeastward along the strike of the 2021 earthquake until it connects with the Flores back-arc thrust (Figure 2; Figure 3a). This coincides with the Kalaotoa Fault identified by (Supendi et al., 2022) as the source of the 2021 earthquake.

5. Some Implications Based on the Broad-Scale Kinematic Model Results

The relative slip rates across the block boundaries between the adjacent blocks and the Euler rotation rate of each block derived from our best-fit model are shown in Figure 3 and Table S2 of Supporting Information S1, respectively. We compared our estimated Euler vectors with the results from previous studies, as summarized in Table S2 of Supporting Information S1. To understand the slip partitioning mechanism, we also decompose slip rates into normal and parallel components (Figure 5).

Most of our results show some agreement with previous estimates, and our more comprehensive datasets give better constraints and smaller uncertainties. On the other hand, there are many areas that still lack enough GPS measurements to provide well-constrained block velocities, in which case the uncertainties are considerable. The Yapen fault zone (YFZ), as expressed in the Biak Basin, actually consists of two parallel, active sinistral faults striking WNW-ESE and separated by a 30 km zone of complex faulting (Memmo et al., 2013). The GPS sites on Yapen Island (POM2 and YAPE) are affected by this complex internal deformation on the island, causing the relatively large modeling residuals at these two sites. In addition, according to the earthquake distribution

(Figure 2) and focal mechanisms (Figure 6), a dextral strike-slip fault extends from Yapen Island to the Lowlands fault zone, forming an active strike-slip deformation zone at the northeast corner in our CEND block, which drives the slip at the north Lowlands fault zone but is not involved in the block modeling since there are no GPS observations to constrain this unmapped strike-slip fault (Figure 3). Hence, we exclude from our analysis the GPS site WREN located near this possible active boundary, to avoid having NW-SE motion on this fault influence the block modeling (Figure 2; Figure 6). In our model, the Yapen fault and Tarera-Adiuna fault are highly active with 36.9 ± 3.9 and 61.3 ± 1.4 mm/yr predominantly sinistral slip, respectively, consistent with the existence of local extensional structures (Charlton, 2000, 2010; Cloos, 2005). Our estimated relative motion rate along the Tarera-Adiuna fault is consistent with the early seismic study of McCaffrey and Abers (1991), which suggested the Tarera-Adiuna fault zone accommodates ~ 60 mm/yr of sinistral motion.

5.1. Kinematics for Three Triple Junction Systems in the Model

Along the eastern boundary of the SERA block, the kinematic scenario shows a transition from thrusting to normal faulting, marked by its intersection with the highly active sinistral Tarera-Adiuna Fault which separates the Seram from the Aru Trough. The Banda block shares the same boundary as the SERA block, indicating 23.8 ± 1.2 mm/yr of sinistral slip rate along the Kawa Shear Zone. This sinistral slip continues along the Banda Detachment with a small component of normal slip (~ 12 mm/yr). The Bird's Head Block rotates anticlockwise relative to the Australian Plate at a rate of $2.82 \pm 0.11^\circ/\text{Myr}$, resulting in an average 26.7 ± 1.3 mm/yr of south-westward motion that is accommodated by the Tarera-Adiuna fault to the south, and contributes to convergence along the Seram Trough (Figure 4; Figure 5). The Tarera-Adiuna Fault intersects the outer Banda Arc where the Seram and Aru Troughs meet, accommodating a shift in footwall movement from SW (i.e., convergent) to NE (i.e., divergent) motion relative to the Australian plate with an average rate of ~ 25.1 mm/yr. This extensional movement is consistent with the recorded focal mechanisms (Figure 3) and also provides kinematic evidence for the Spakman and Hall (2010) rollback model in the Banda arc, explaining the formation of this spoon-shaped embayment. The SERA, BRHD, and AUST blocks comprise a triple junction system. The three boundaries consist of a compressional Seram Trench, an extensional Aru Trough, and a sinistral strike-slip Tarera-Adiuna Fault, following the Ridge–Trench–transform Fault type put forward by McKenzie and Morgan (1969) and showing high stability based on the estimated relative velocity vectors (Kearey et al., 2013).

In the PNG area, comparing with Koulali et al. (2015), in addition to the GPS data derived from Koulali et al. (2015), we added the GPS velocities from Wallace et al. (2014) and Biemiller et al. (2020) into the inversion. These additional velocities are mainly distributed around the Huon Peninsula, Papuan Peninsula, and D'Entrecasteaux Islands. Although some of the tectonic complexity of this region results in internal block deformation not associated with block boundary locking, our model provides a good fit for the GPS observations in Southeastern PNG. This suggests that most of the deformation is associated with the rotation and locked boundaries of the blocks in our model. Also, our results for block boundary slip are mostly consistent with previous studies on the crustal block rotation and strain associated with fault locking (Biemiller et al., 2020; Wallace et al., 2014). For example, the rapid clockwise rotation of the south Bismarck plate results in a rapid escalation of convergence rate along the Ramu-Markham fault: from 3.4 ± 0.3 mm/yr at the northern end of the west ADBL boundary to 25.2 ± 1.7 mm/yr at the Huon Peninsula area, and it increases further to 45.5 ± 1.5 mm/yr at the junction of the NBT and Ramu-Markham fault, which is consistent with Wallace et al. (2004) (Figure 3 and Figure 4). The convergence rate also increases along the New Britain Trench, reaching 149.6 ± 3.3 mm/yr at 152.8°E , which is consistent with Wallace et al. (2014) indicating the highest convergence on the NBT is up to ~ 150 mm/yr. The estimation of the pole of rotation of the Woodlark block with respect to the Australian Plate is at longitude 147.82°E , latitude -9.19°S with an anticlockwise rotation of $2.61 \pm 0.06^\circ/\text{Myr}$, resulting in decreasing extensional rates from 43.4 ± 0.9 mm/yr at 156.8°E to 10.4 ± 0.3 mm/yr at 149.8°E along the Woodlark Rift, with continued reduction in slip rate along the Owen Stanley fault zone to as low as ~ 1 mm/yr. Again, these are close to the estimated slip rates along the same faults in Wallace et al. (2014) using the Trobriand Block/Australian Plate Euler pole rotation. Wallace et al. (2014) studied the Woodlark area in more detail, subdividing the WDBL of this paper into six smaller microblocks, including a Trobriand Block and the Solomon Sea and Woodlark Plates. While this finer microblock configuration reveals important details of the extension and continental breakup occurring in this part of PNG, our results for the larger-scale block movement and fault slip are very similar to those of Wallace et al. (2014). For example, the Trobriand block in Wallace et al. (2014) is the largest of the six microblocks, accounting for over 60% of our WDBL, and the estimated pole of rotation of our WDBL is

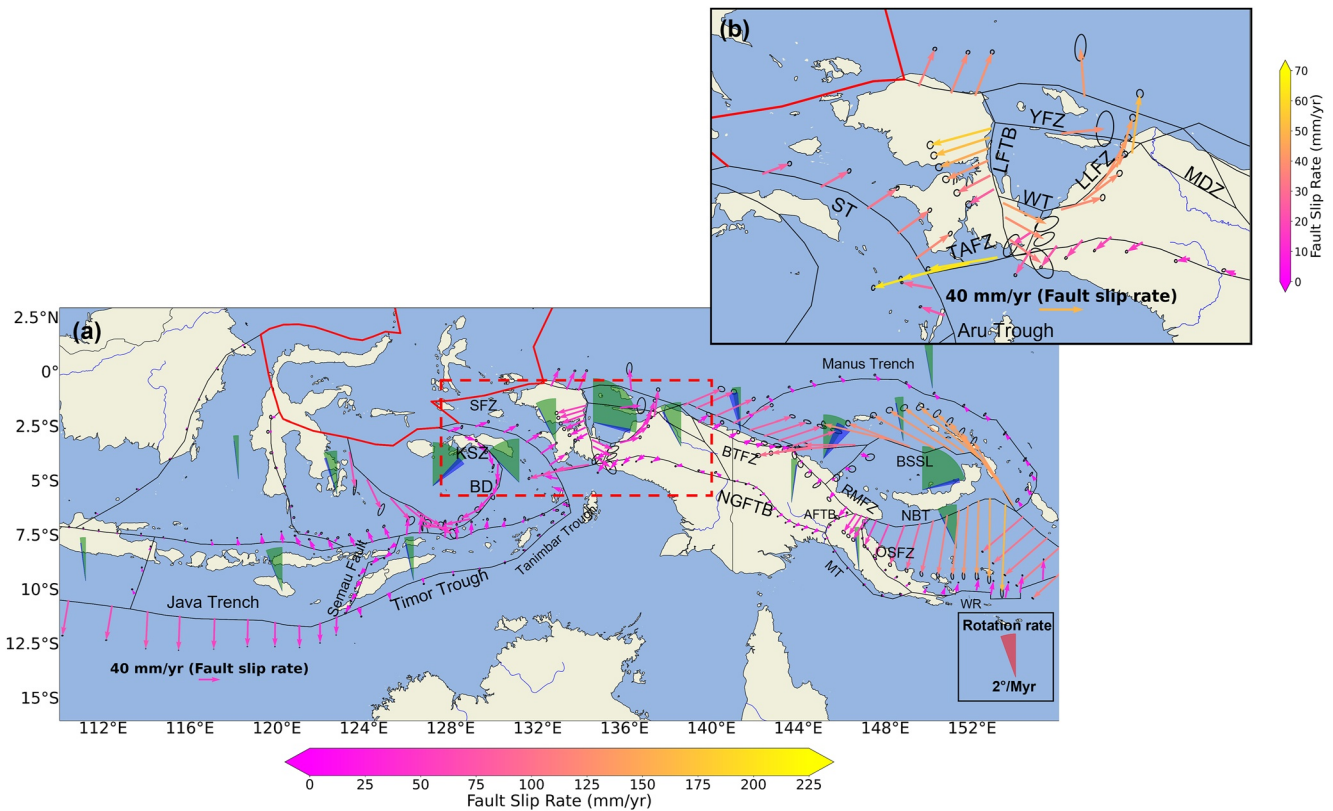


Figure 4. (a) Relative fault slip vectors across the active block boundaries with 95% error ellipses. The abbreviation of each active fault has been defined and indicated in Figure 1. The magnitude of the slip vectors is proportional to the size of the arrows. Arrows show the movement of a hanging wall relative to a footwall, and the tails of arrows are located on the hanging wall. The green wedges represent the block rotation rate with respect to the Australian Plate. If the wedge is open to the west, it represents the anticlockwise rotation of the block, or conversely (scale is located at the lower right corner in red). The blue wedges indicate the uncertainties of the rotation rates. Since the YAPE, TABL, and MABL blocks only contain one global positioning system (GPS) observation, the rotation estimates have significant uncertainties. Therefore the results are not shown here. For the northern boundary of the Yapen fault, we chose to use the estimated slip vector with the smallest uncertainty located both near the GPS velocity in the Yapen block and related earthquake slip vectors to indicate the deformation of the Yapen fault northern boundary. The estimated location of the Euler pole for each block is given in Table S2 of Supporting Information S1. (b) The inset figure corresponds to the red dashed rectangle area in panel a, showing the close-up view of the estimated slip vectors in Western New Guinea. Note that the color scale is different for each figure.

consistent with that of Wallace et al.'s (2014) Trobriand block, $-2.69 \pm 0.13^\circ/\text{Myr}$ with the pole at the longitude 147.85°E , latitude -9.54° (Table S2 of Supporting Information S1).

The pre-rift evolution of the Woodlark Basin includes arc volcanism, subduction, and arc-continent collision, which was partially accommodated by the Moresby Trough (MT; Baldwin et al., 2012). As the southwest boundary of the PPBL Block, we estimate a convergence on the order of 4 mm/yr across the MT. While the Aure Fold and Thrust Belt (AFTB) is a region of diffuse seismicity likely reflecting activity on the distribution of small faults, we have represented it as a single fault that separates the Eastern Highlands and the Papuan Peninsula blocks (ENGH and PPBL, respectively). Our estimate for relative motion on the AFTB increases from 5.7 ± 0.9 at its southern end, where it merges with the MT, to 6.5 ± 0.6 mm/yr at its northern end, where it intersects the RMFZ.

We note our kinematic model results in extremely high relative velocity along the Weitin Fault, at the boundary between the North and South Bismark blocks (NBBL and SBBL, Figures 1 and 3a). Previous studies have also resulted in high slip rates along this transform fault zone, with Tregoning et al. (1999) obtaining 130 mm/yr, Wallace et al. (2004) 140 mm/yr, and Koulali et al. (2015) 144 mm/yr. The sinistral relative block motion we obtain is 145.7 ± 3.1 mm/yr but could be higher (up to ~ 171 mm/yr) if include site RABL in the analysis (Tregoning et al., 1998a; Figure S1 of Supporting Information S1). The site RABL was not included in our analysis because it is on a highly active volcano and its velocity may be strongly influenced by volcanic processes unrelated to plate motion. However, the influence of the volcano activity on site RABL has not been quantified,

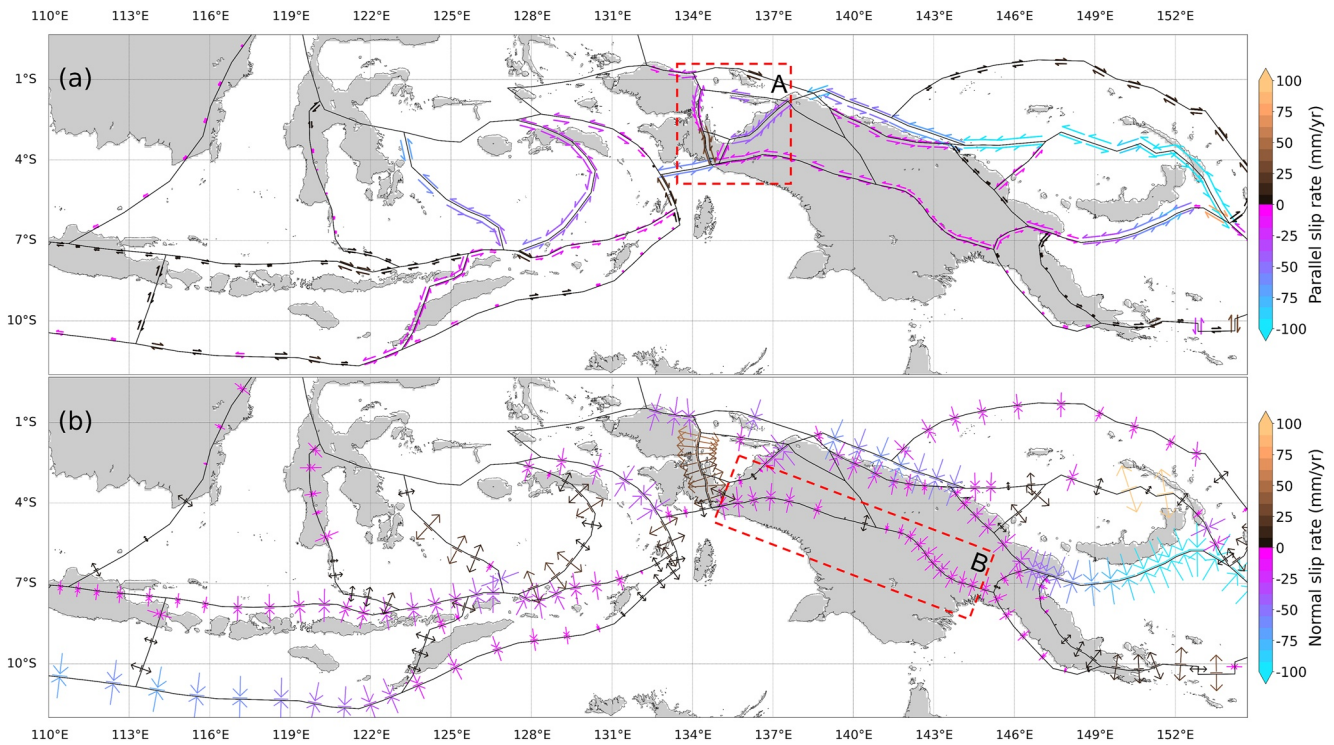


Figure 5. (a) The fault-parallel component of relative fault slip rates; positive value represents dextral strike-slip, and a negative value represents sinistral strike-slip (b) The fault-normal component of relative fault slip rate; positive value represents an extension, and a negative value represents compression. The value of the slip rate is logarithmically proportional to the size of the symbol for better visualization. The dashed rectangles A and B represent the area that will be further discussed in Figures 6 and 7, respectively.

so we cannot exclude the possibility that it is small, and that the velocity of RABL is reflecting an even higher slip rate along the Weitin Fault of 171 mm/yr.

This compares with 50–57 mm/yr along the Queen Charlotte Fault offshore western British Columbia, described by Brothers et al. (2020) as having “the fastest rate for a continent-ocean strike-slip fault on Earth”, or 42 mm/year for the Palu Koro Fault in Indonesia (Socquet et al., 2006), which is also regarded as having a very high slip rate. While some ocean transform faults, such as some relatively short transform segments along the East Pacific Rise (Lonsdale, 1978) or near the northern edge of the Tonga Trench, may have higher slip rates, we believe the Weitin fault has by far the highest slip rate of any major (i.e., greater than 200 km length) transform fault on earth. This is possible even if we allow that accommodation of the relative block motion may be shared with other small-scale parallel faults in New Ireland (Lindley, 2006). The Weitin fault experienced an overlapping rupture in two recent major earthquakes in 2000 and 2019 (Mw 8.0 and 7.7, respectively), and Ghasemi et al. (2020) have shown that high seismicity is commensurate with a very high slip rate.

5.2. Deformation Rates on the Sunda-Banda Subduction System

From the Java Trench to the Timor Trough, the estimated relative slip rates show an eastward decreasing trend, from 65.1 ± 0.3 mm/yr (at 112.4°E) to 10.9 ± 0.3 mm/yr (at 126.7°E). The direction of the slip rates across this boundary shows a sudden change from southward to southeastward, a transition which is accommodated by and coincides with the intersection with extensional/sinistral motion on the Semau Fault (Figure 4). This progressive change in the relative velocity and slip azimuth is also apparent in the back-arc region, where it has the opposite sense to the change in motion on the megathrust. The slip rate on the Flores back-arc thrust gradually increases eastward from 4.8 ± 0.5 mm/yr at 110.4°E to 29.9 ± 2.0 mm/yr at 126.5°E , with the change again dictated by its intersection with the Semau Fault (Figure 4). Furthermore, in the east, the relative velocity along the back-arc changes to a more eastward direction, indicating a shear component of motion, which is consistent with the earthquake focal mechanisms as shown in Figure S3b of Supporting Information S1. The relative slip rates we

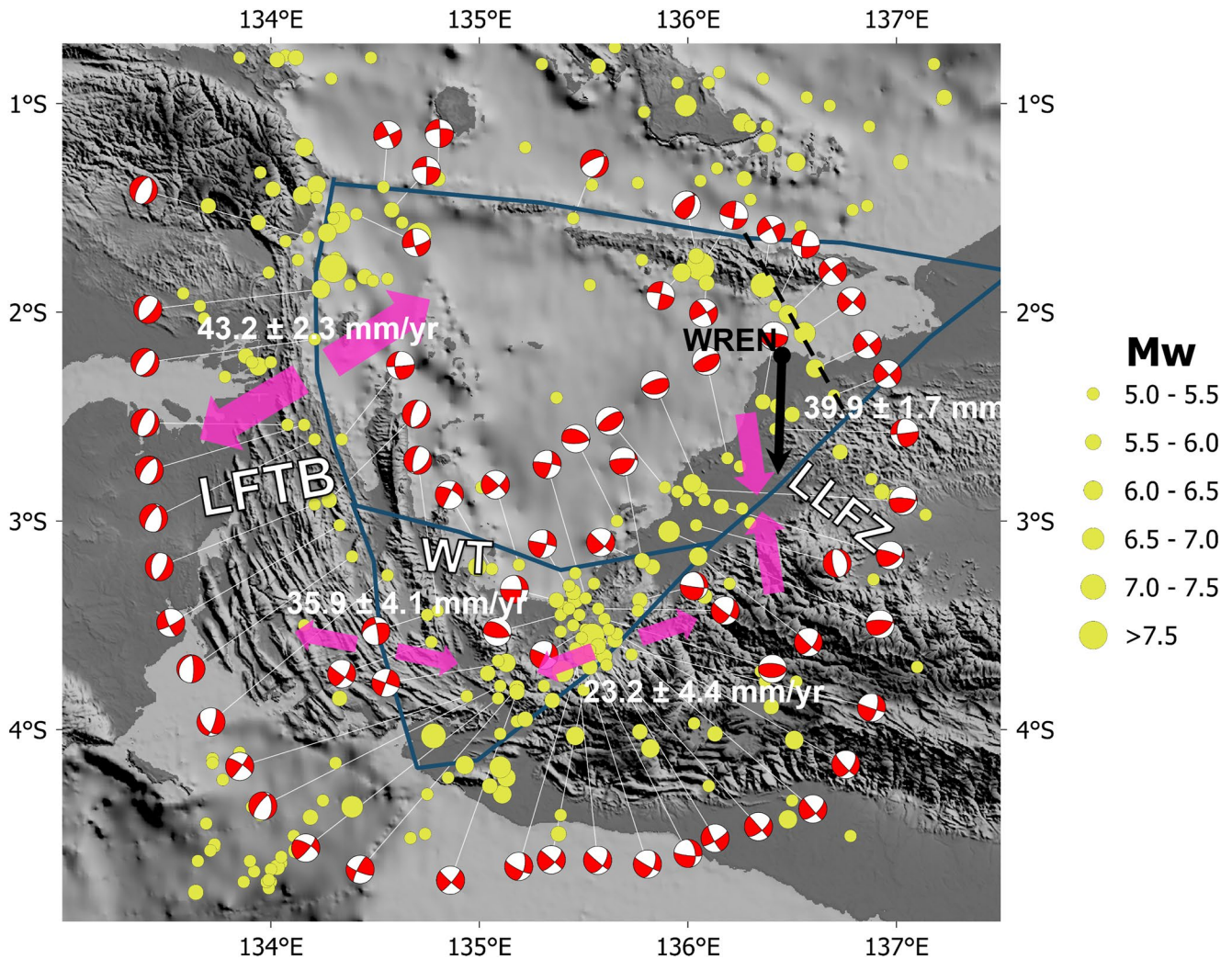


Figure 6. The distribution of the earthquake focal mechanisms in Cenderawasih Bay region (rectangle area A in Figure 5a). The seismicity data are derived from the global centroid moment tensor catalog with depth less than 50 km and $M_w > 5$ from 1976 to 2021. The purple arrows show the undergoing oblique compression and extension along the active block boundaries represented by the solid line. The black solid arrow represents the global positioning system velocity WREN, which was excluded in the inversion, and the dashed line represents the locus of the unmapped boundary based on the seismicity distribution. The bathymetry data are from <https://www.gebco.net/>. The modeled earthquake slip vectors for this region are shown in Figure S3c of Supporting Information S1.

obtained along the Sunda-Banda megathrust and Flores back-arc thrust are slightly smaller than those estimated in Koulali et al. (2016), mainly because of the GPS velocities we newly applied on Java and Timor Island, which have slightly slower velocities, and the revised block boundaries for SUND, EMAK, and WMAK blocks. In the TIMO block, our two new GPS observations (stations DILI and SAME) first reveal the deformation in East Timor and better constrain the deformation rate on the boundary of the block. Compared with the motion of the TIMO block suggested by Koulali et al. (2016), our block scenario decreases the NRMS/WRMS value significantly, from 4.05/2.14 to 2.48/1.34.

5.3. Geodetic Implications for the Tectonic Evolution of Cenderawasih Bay

As mentioned above, the origin of Cenderawasih Bay is the subject of ongoing debate. Our kinematic model provides some geodetic constraints for the development of Cenderawasih Bay by quantifying the movement on the active block boundaries. The decomposition of relative block motion depicted in Figure 5 highlights the opposing tectonic regimes on the west and east boundaries (Lengguru and Lowlands fault zones) of CEND (Figure 5). The relative movement along the west boundary shows significant partitioning of extensional deformation decreasing southward, from 50.3 ± 1.8 to 25.8 ± 1.7 mm/yr, supported by the recorded focal mechanisms

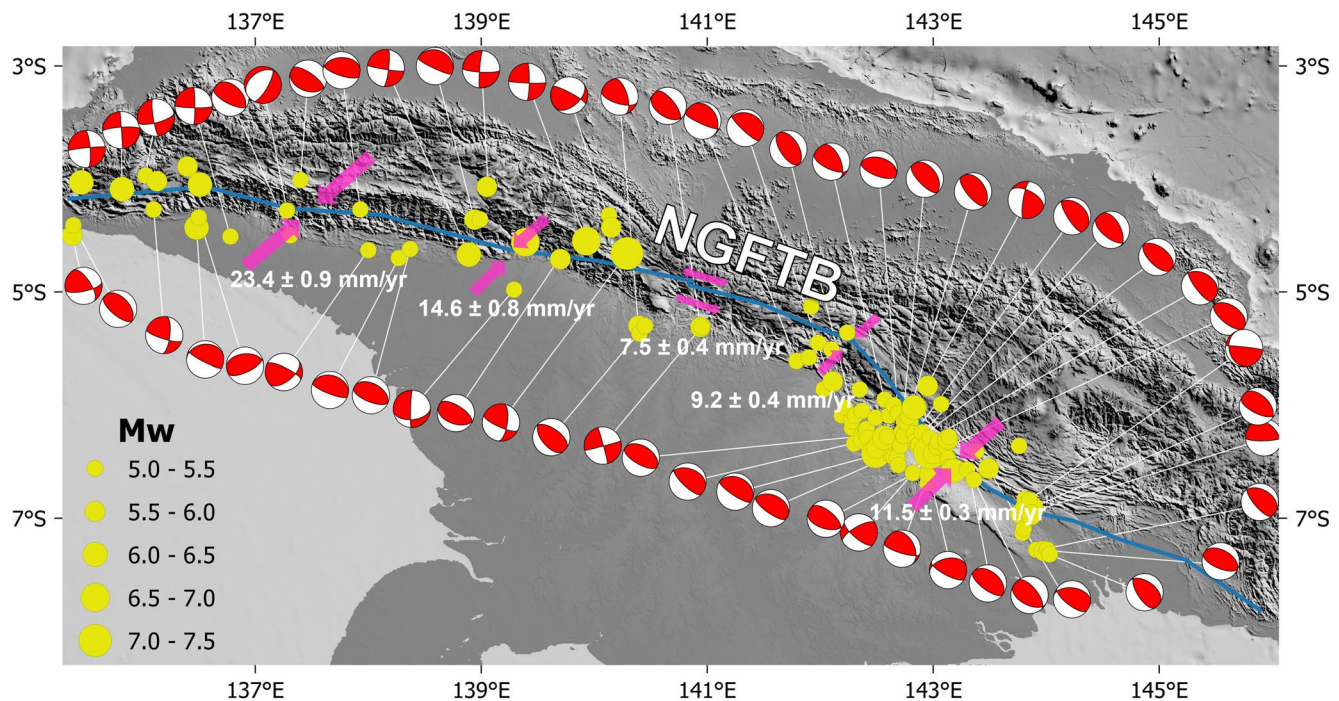


Figure 7. The distribution of the earthquake focal mechanisms in Cenderawasih Bay region (rectangle area B in Figure 4b). The seismicity data are derived from the GCMT catalog, using events with depth less than 50 km and magnitude larger than five from 1976 to 2021. The arrows show the undergoing oblique compression and sinistral strike-slip along the active block boundaries represented by the solid line.

in this area (Figure 6). This dramatic extension is interpreted as a very recent tectonic movement, probably since the Pleistocene, which is coeval with the onset of the transtensional regime of the Tarera-Adiuna fault and the Paniai fault leading to the collapse of Cenderawasih Bay (Bailey et al., 2009).

The nature of this extension may be closely related to the evolution of Cenderawasih Bay and is a matter of some debate. One hypothesis involves tectonic escape caused by the rollback of the Seram Trench and is associated with the sinistral movement on the Tarera-Adiuna strike-slip fault. The other hypothesis is the anticlockwise rotation of the Bird's Head block (BRHD) driven by the convergence between the Australian and Pacific Plates (i.e., the oblique convergence between BRHD and the Pacific Plate in the north pushes the top of the BRHD westward, while the oblique convergence with the Australian Plate in the south pushes the bottom of BRHD eastward) (Charlton, 2000, 2010). Our kinematic evidence is more consistent with the second hypothesis, considering the estimated extension rate on the northern part of the Lengguru fault zone is significantly larger than that on the southern part. However, the anticlockwise rotation rate ($2.82 \pm 0.11^\circ/\text{Myr}$) of the Bird's Head block derived from our kinematic model is much smaller than that estimated by Charlton (2000, 2010), which suggests that the rotation of the Bird's Head block is not the only driver of the Cenderawasih sphenochasm formation. The significant volume of sediments accumulated in Cenderawasih Bay and Waipoga Basin also indicates that the evolution of the embayment should have started before ~ 12 Ma rather than the Pliocene opening of the bay suggested by Babault et al. (2018).

The convergence rate on the northern Lowlands fault zone is larger than that on the southern part, whilst the fault-parallel rates are uniform along the entire fault zone, which has an average sinistral strike-slip rate of 36.5 ± 1.7 mm/yr (Figure 5a and 5b). This is consistent with the distribution of thrust and strike-slip earthquake focal mechanisms, as well as with the tectonic setting (Figure 1 and Figure 6). This uniform southwestward fault-parallel translation of blocks TABL and CEND provides geodetic evidence supporting the southwestward drift hypothesis for the formation of the Cenderawasih Bay sphenochasm put forward by François et al. (2016), which suggested that the Weyland overthrust has migrated 25-km-southwestward during the Late Miocene (Babault et al., 2018). This southwestward translation is consistent with the dextral strike-slip motion on the southwestern part of the Lengguru fault zone with an average slip rate of 24.1 ± 3.9 mm/yr, which is supported by geological and seismic evidence (Figure 6; Babault et al., 2018; Cloos, 2005; Dow & Sukanto, 1984; François

et al., 2016; Pubellier & Ego, 2002; Stevens et al., 2002), as well as by the sinistral motion on the Lowlands fault (Figure 7; Babault et al., 2018; Cloos, 2005; Dow & Sukanto, 1984; François et al., 2016; Pubellier & Ego, 2002; Stevens et al., 2002). Extensional earthquakes are distributed all along the entire Lengguru fault zone, but the dextral strike-slip earthquakes are primarily concentrated in the southwestern part. This seismicity pattern is in excellent agreement with our kinematic model. We deduce that the WSW drift of blocks CEND and TABL is accommodated mainly by the sinistral slip along the entire Lowlands fault zone, but is also partially accommodated by the dextral slip on the southern part of the Lengguru fault. The shift of the strike-slip style and the northward increasing extension rate on the Lengguru fault zone indicate that both driving mechanisms (Bird' Head rotation and southwestward drift of the Weyland overthrust) have been and still are active, contributing to the development of Cenderawasih Bay. We note that the sparsity of the GPS data in the TABL block results in large uncertainties on the estimated relative slip rates along the boundary faults.

5.4. Tectonic Regime Change Along the New Guinea Fold-And-Thrust Belt

The NGFTB covers much of the island of New Guinea, and our model predicts relative velocities across this belt that undergoes two different transitions from west to east. The relative motion along the NGFTB decreases from 25.8 ± 0.9 mm/yr at the western end of the belt to 7.1 ± 0.4 mm/yr at 141.2°E , then increases to 12.3 ± 0.6 mm/yr at the eastern end of the belt (Figure 6). Additionally, the direction of relative motion also exhibits a variation, from southwestward to westward then back to southwestward again, indicating a transition from oblique thrust to sinistral strike-slip and back to oblique thrust that is consistent with the observed earthquake focal mechanisms (Figure 7).

The NGFTB formed because of the diachronous collisional orogenesis resulting from the Melanesian arc-continent oblique collision that occurred in the Late Oligocene-Miocene, beginning from the west and propagating to the east (Baldwin et al., 2012; Cloos, 2005). According to our decomposed relative motion results, the average convergence of the western part of the NGFTB (west of longitude 141°E) is ~ 10.6 mm/yr. The relative fault-normal motion decreases from 19.5 ± 0.6 to 1.4 ± 1.2 mm/yr toward the east. The average fault-parallel velocity is 13.5 ± 0.9 mm/yr (Figure 5). In the east segment, the average convergence is ~ 8.5 mm/yr with an increase of relative fault-normal motion from 2.2 ± 0.7 to 9.0 ± 0.5 mm/yr toward the east, and the average fault-parallel velocity is ~ 5.7 mm/yr. Geologic evidence indicates that the shortening across the western NGFTB may have already ceased at ~ 4 Mya, and the eastern segment is undergoing a shortening stage similar to that of the western segment prior to 4 Mya, implying that the convergence rate of the western NGFTB should be lower than that of the eastern NGFTB (Baillly et al., 2009; Baldwin et al., 2012; Cloos, 2005; Hill et al., 2003). However, in our estimation, both fault-parallel and fault-normal rates on the western segment of the NGFTB are larger than those on the eastern segment, which suggests that the western NGFTB also accommodates oblique shortening from some other tectonic activity. This seems likely, considering that the westernmost NGFTB conjuncts with multiple active diffuse fault zones, including the Tarera-Adiuna fault zone, Lowlands fault zone, and Paniai fault zone, which accommodate transtensional deformation from the rotation of the Bird's Head block and the southwestward drift of Weyland overthrust (François et al., 2016; Stevens et al., 2002; Watkinson & Hall, 2017). The relatively large oblique motion on the western end of the NGFTB is more likely the consequence of the combination of the sinistral movement along these intersecting fault zones rather than the collisional orogenesis. In addition, the low convergence rate we obtained for the center NGFTB that increases toward the east is consistent with prior studies, in the sense that the east NGFTB is still active. However, in the central section, our geodetic results suggest that the NGFTB is still undergoing slow convergence rather than having ceased shortening completely.

6. Conclusions

This study is the first attempt to give the entire Indonesia-Australia-New Guinea collision zone a broad quantitative interpretation by utilizing over 200 available GPS observations and 492 earthquake slip vectors. As one of the most tectonically complicated and seismically active regions globally, the kinematic framework for the deformation in this boundary zone has hitherto been piecemeal. The new GPS velocity field has filled important knowledge gaps in the Banda Sea and West New Guinea areas and updated previous studies in the Sunda-Banda arc and Papua New Guinea. Our broad-scale kinematic model emphasizes the motion change along the active boundary faults, which is in some cases quite pronounced, thereby enhancing our understanding of the evolution of some large tectonic structures. Although the estimated kinematic results of the first-order block properties

presented in this study may not account for some localized effects that may require more detailed microblock parameterization, we believe they are useful for understanding the broad-scale tectonics and provide a useful framework for further, more detailed studies.

We suggest that the western New Guinea Fold-and-Thrust Belt accommodates larger convergence (between 4 and 18 mm/yr) than the eastern segment of NGFTB (between 3 and 11 mm/yr), which is mainly caused by the stress transfer from the highly active Tarera-Aiduna, Lowlands and Paniai fault zones. The combined effect of these active faults is diminished eastward, and the shortening accommodated on the NGFTB becomes the only driving mechanism of the ongoing convergence, increasing from the middle segment (~138°E to 142°E) to the eastern NGFTB (~142°E to 144°E). Hence, we can observe a double shift in the tectonic regime along this ~2,000 km highland belt. The estimated rotation rate of the Bird's Head block and the slip style transitions along the Lowlands and Lengguru fault zones provide the geodetic evidence that the formation of the Cenderawasih Bay sphenochasm is due to both the interaction of both Bird's Head rotation and the southwestward drift of the Weyland Overthrust, and that both these mechanisms continue to be active.

One of the important reasons for developing our kinematic block model is to guide the assessment of seismic hazards. Recent seismic hazard assessments for both Indonesia (Irsyam et al., 2020) and PNG (Ghasemi et al., 2016, 2020) make extensive use of such tectonic block models to refine estimates of seismic hazard. In both cases, these have revealed areas where the hazard level was significantly higher than earlier assessments done without the benefit of detailed kinematic block models. For example, the high rate and dramatic eastward increase in the rate of convergence of the Ramu-Markham Fault, which passes near PNG's second-largest city, Lae, confirms the very high seismic hazard inferred by Ghasemi et al. (2020), based on the earlier kinematic block models of Wallace et al. (2014) and Koulali et al. (2015).

The plausible kinematic scenario presented by our model is consistent with other seismic and geological evidence, whereas we also note that some blocks are not fully explained; the relatively large χ^2 values for some blocks imply the potential existence of other micro-blocks in these regions. The lack of observations in some blocks leads to large uncertainty on some estimated block motions. The locking coefficient of the block-bounding active faults in the West New Guinea region is also largely unresolved due to the lack of nearby GPS observations. Therefore, to better investigate the potential existence of active structures and quantify the seismic hazard posed by these structures, and provide the local populations with information about the likely nature of future earthquakes, more dense, long-term, and continuous GPS observations are essential.

Acknowledgments

We sincerely appreciate Rui Fernandes, who participated in the GPS surveys on Timor Island. With his help, we obtained the GPS data from the SAME station. MSM was funded by National Science Foundation (NSF) Grant EAR-1250214. The authors thank the Instituto do Petróleo e Geologia (IPG) of Timor-Leste, without whose support this work would not have been possible. Additional thanks to UNAVCO for the instrumentation provided to IPG and ANU at the SAME, DILI stations and the raw GPS RINEX data for Irian Jaya 2002, 2004 (McCaffrey, 2002, 2005). Furthermore, we are grateful to Dr. Achraf Koulali for his instruction on the TDEFNODE software. We also thank Robert W. King for providing GAMIT/GLOBK (<http://geoweb.mit.edu/gg/>) and Rob McCaffrey for providing TDEFNODE (<https://robmccaffrey.github.io/TDEFNODE/TDEFNODE.html>). Open access publishing facilitated by Australian National University, as part of the Wiley - Australian National University agreement via the Council of Australian University Librarians.

Data Availability Statement

GPS velocities utilized in this study and the earthquake focal mechanisms picked for calculating the slip vectors are given in supporting information, including the two new GPS measurements in East Timor. The raw GPS data of our reprocessed velocities (McCaffrey, 2002, 2005) and two new velocities (SAME and DILI) are provided and archived via UNAVCO, Inc; all of them can be downloaded on request from the UNAVCO data porta (<https://www.unavco.org/data/gps-gnss/data-access-methods/dai1/campaign.php>). The corresponding DOI links of the RINEX files are <https://doi.org/10.7283/T5765CDW> and <https://doi.org/10.7283/T5BZ643V> for the reprocessed velocities; <https://doi.org/10.7283/XZNW-N019>, <https://doi.org/10.7283/18YM-D875>, and <https://doi.org/10.7283/KVQF-TP50> for the new acquisitions. The control and input files for the modeling we performed in this study are available in the Supporting Information S1.

References

- Abers, G., & McCaffrey, R. (1988). Active deformation in the New Guinea fold-and-thrust belt: Seismological evidence for strike-slip faulting and basement-involved thrusting. *Journal of Geophysical Research*, 93(B11), 13332–13354. <https://doi.org/10.1029/jb093ib11p13332>
- Abers, G. A., & McCaffrey, R. (1989). Active tectonics and seismicity of new Guinea. Massachusetts Institute of technology.
- Abers, G. A., & McCaffrey, R. (1994). Active arc-continent collision: Earthquakes, gravity anomalies, and fault kinematics in the Huon-Finisterre collision zone, Papua New Guinea. *Tectonics*, 13(2), 227–245. <https://doi.org/10.1029/93tc02940>
- Aki, K., & Richards, P. G. (1980). Quantitative seismology: Theory and methods. *New York*, 801.
- Alvarez, W., Coccozza, T., & Wezel, F. C. (1974). Fragmentation of the Alpine orogenic belt by microplate dispersal. *Nature*, 248(5446), 309–314. <https://doi.org/10.1038/248309a0>
- Babault, J., Viaplana-Muzas, M., Legrand, X., Van den Driessche, J., González-Quijano, M., & Mudd, S. M. (2018). Source-to-sink constraints on tectonic and sedimentary evolution of the Western central range and Cenderawasih bay (Indonesia). *Journal of Asian Earth Sciences*, 156, 265–287. <https://doi.org/10.1016/j.jseas.2018.02.004>

- Bailly, V., Pubellier, M., Ringenbach, J., Sigoyer, J. D., & Sapin, F. (2009). Deformation zone jumps in a young convergent setting: the Lengguru fold-and-thrust belt, New Guinea Island. *Lithos*, *113*(1–2), 306–317. <https://doi.org/10.1016/j.lithos.2009.08.013>
- Baldwin, S. L., Fitzgerald, P. G., & Webb, L. E. (2012). Tectonics of the new Guinea region. *Annual Review of Earth and Planetary Sciences*, *40*(1), 495–520. <https://doi.org/10.1146/annurev-earth-040809-152540>
- Barondess, S., & Utku, S. (1963). Computation of weighted root mean square of path length changes caused by the deformations and Imperfections of rotational Paraboloidal antennas.
- Biemiller, J., Boulton, C., Wallace, L., Ellis, S., Little, T., Mizera, M., et al. (2020). Mechanical implications of creep and partial coupling on the world's fastest slipping low-angle normal fault in southeastern Papua New Guinea. *Journal of Geophysical Research: Solid Earth*, *125*(10), e2020JB020117. <https://doi.org/10.1029/2020jb020117>
- Bird, P. (2003). An updated digital model of plate boundaries. *Geochemistry, Geophysics, Geosystems*, *4*(3). <https://doi.org/10.1029/2001gc000252>
- Bock, Y., Prawirodirdjo, L., Genrich, J., Stevens, C., McCaffrey, R., Subarya, C., et al. (2003). Crustal motion in Indonesia from global positioning system measurements. *Journal of Geophysical Research*, *108*(B8), 2367. <https://doi.org/10.1029/2001jb000324>
- Brothers, D. S., Miller, N. C., Barrie, J. V., Haussler, P. J., Greene, H. G., Andrews, B. D., et al. (2020). Plate boundary localization, slip-rates and rupture segmentation of the Queen Charlotte Fault based on submarine tectonic geomorphology. *Earth and Planetary Science Letters*, *530*, 115882. <https://doi.org/10.1016/j.epsl.2019.115882>
- Carter, D. J., Audley-Charles, M. G., & Barber, A. (1976). Stratigraphical analysis of island arc—Continental margin collision in eastern Indonesia. *Journal of the Geological Society*, *132*(2), 179–198. <https://doi.org/10.1144/gsjgs.132.2.0179>
- Charlton, T. (2000). Tertiary evolution of the eastern Indonesia collision complex. *Journal of Asian Earth Sciences*, *18*(5), 603–631. [https://doi.org/10.1016/s1367-9120\(99\)00049-8](https://doi.org/10.1016/s1367-9120(99)00049-8)
- Charlton, T. R. (2010). The Pliocene-recent anticlockwise rotation of the Bird's Head, the opening of the Aru Trough—Cendrawasih bay sphenochasm, and the closure of the Banda double arc.
- Chase, C. G. (1978). Plate kinematics: The Americas, East Africa, and the rest of the world. *Earth and Planetary Science Letters*, *37*(3), 355–368. [https://doi.org/10.1016/0012-821x\(78\)90051-1](https://doi.org/10.1016/0012-821x(78)90051-1)
- Chen, H., Cui, Z., Zhu, R., & Gao, X. (2010). Evaluating the effects of differences in group abilities on the Tucker and the Levine observed-score methods for common-item nonequivalent groups equating.
- Chen, K., Milliner, C., & Avouac, J. P. (2019). The Weitin Fault, Papua New Guinea, ruptured twice by Mw 8.0 and Mw 7.7 earthquakes in 2000 and 2019. *Geophysical Research Letters*, *46*(22), 12833–12840. <https://doi.org/10.1029/2019gl084645>
- Cloos, M. (2005). *Collisional delamination in New Guinea: The geotectonics of subducting slab breakoff* (Vol. 400). Geological Society of America.
- Cronin, V. (2004). A draft primer on focal mechanism solutions for Geologists, in “on the Cutting edge” Workshop on teaching structural geology in the 21st century. Science Education Resource center, Carleton College, 14.
- Cummins, P. R., Pranantyo, I. R., Pownall, J. M., Griffin, J. D., Meilano, I., & Zhao, S. (2020). Earthquakes and tsunamis caused by low-angle normal faulting in the Banda Sea, Indonesia. *Nature Geoscience*, *13*(4), 312–318. <https://doi.org/10.1038/s41561-020-0545-x>
- Das, S. (2004). Seismicity gaps and the shape of the seismic zone in the Banda Sea region from relocated hypocenters. *Journal of Geophysical Research*, *109*(B12), B12303. <https://doi.org/10.1029/2004jb003192>
- Davies, H., & Smith, I. (1971). Geology of eastern Papua. *The Geological Society of America Bulletin*, *82*(12), 3299–3312. [https://doi.org/10.1130/0016-7606\(1971\)82\[3299:goep\]2.0.co;2](https://doi.org/10.1130/0016-7606(1971)82[3299:goep]2.0.co;2)
- DeMets, C., Gordon, R. G., Argus, D., & Stein, S. (1990). Current plate motions. *Geophysical Journal International*, *101*(2), 425–478. <https://doi.org/10.1111/j.1365-246x.1990.tb06579.x>
- DeMets, C., Gordon, R. G., Argus, D. F., & Stein, S. (1994). Effect of recent revisions to the geomagnetic reversal time scale on estimates of current plate motions. *Geophysical Research Letters*, *21*(20), 2191–2194. <https://doi.org/10.1029/94gl02118>
- Dewey, J. F., Pitman, W. C., III, Ryan, W. B., & Bonnin, J. (1973). Plate tectonics and the evolution of the Alpine system. *The Geological Society of America Bulletin*, *84*(10), 3137–3180. [https://doi.org/10.1130/0016-7606\(1973\)84<3137:ptateo>2.0.co;2](https://doi.org/10.1130/0016-7606(1973)84<3137:ptateo>2.0.co;2)
- Di Piazza, A., Piazza, M. C., & Vitale, G. (2016). Solar and wind forecasting by NARX neural networks. *Renewable Energy and Environmental Sustainability*, *1*, 39. <https://doi.org/10.1051/rees/2016047>
- Dow, D., & Sukanto, R. (1984). Western Irian Jaya: The end-product of oblique plate convergence in the late Tertiary. *Tectonophysics*, *106*(1–2), 109–139. [https://doi.org/10.1016/0040-1951\(84\)90224-5](https://doi.org/10.1016/0040-1951(84)90224-5)
- Ekström, G., Nettles, M., & Dziewoński, A. (2012). The global CMT project 2004–2010: Centroid-moment tensors for 13,017 earthquakes. *Physics of the Earth and Planetary Interiors*, *200*, 1–9. <https://doi.org/10.1016/j.pepi.2012.04.002>
- Fitch, T. J. (1970). Earthquake mechanisms and island arc tectonics in the Indonesian-Philippine region. *Bulletin of the Seismological Society of America*, *60*(2), 565–591.
- Fitch, T. J. (1972). Plate convergence, transcurrent faults, and internal deformation adjacent to southeast Asia and the Western Pacific. *Journal of Geophysical Research*, *77*(23), 4432–4460. <https://doi.org/10.1029/jb077i023p04432>
- François, C., de Sigoyer, J., Pubellier, M., Bailly, V., Cocherie, A., & Ringenbach, J.-C. (2016). Short-lived subduction and exhumation in Western Papua (Wandamen peninsula): Co-Existence of HP and HT metamorphic rocks in a young geodynamic setting. *Lithos*, *266*, 44–63. <https://doi.org/10.1016/j.lithos.2016.09.030>
- Genrich, J. F., Bock, Y., McCaffrey, R., Calais, E., Stevens, C. W., & Subarya, C. (1996). Accretion of the southern Banda arc to the Australian plate margin determined by Global Positioning System measurements. *Tectonics*, *15*(2), 288–295. <https://doi.org/10.1029/95tc03850>
- Ghasemi, H., Cummins, P., Weatherill, G., McKee, C., Hazelwood, M., & Allen, T. (2020). Seismotectonic model and probabilistic seismic hazard assessment for Papua New Guinea. *Bulletin of Earthquake Engineering*, *18*(15), 6571–6605. <https://doi.org/10.1007/s10518-020-00966-1>
- Ghasemi, H., McKee, C., Leonard, M., Cummins, P., Moihoi, M., Spiro, S., et al. (2016). Probabilistic seismic hazard map of Papua New Guinea. *Natural Hazards*, *81*(2), 1003–1025. <https://doi.org/10.1007/s11069-015-2117-8>
- Hall, R. (2011). Australia–SE Asia collision: Plate tectonics and crustal flow. *Geological Society, London, Special Publications*, *355*(1), 75–109. <https://doi.org/10.1144/sp355.5>
- Hamilton, W. B., & Indonesia Departemen Pertambangan, United States. Agency for International Development. (1979). *Tectonics of the Indonesian region*. U.S. Govt. Print. Off.
- Harris, R., Vorkink, M. W., Prasetyadi, C., Zobell, E., Roosmawati, N., & Aporthe, M. (2009). Transition from subduction to arc-continent collision: Geologic and neotectonic evolution of Savu Island, Indonesia. *Geosphere*, *5*(3), 152–171. <https://doi.org/10.1130/ges00209.1>
- Hayes, G. (2018). Slab2—A comprehensive subduction zone geometry model: US geological survey data release.
- Herring, T., King, R., Floyd, M., & McClusky, S. (2015). GAMIT reference manual. GPS analysis at MIT GLOBK, Release. *Massachusetts Institute of Technology*, *10*, 6.
- Herring, T., King, R., & McClusky, S. (2010). *Introduction to Gamit/Globk*. Massachusetts Institute of Technology.

- Herring, T., King, R., & McClusky, S. (2015). GLOBK reference manual. *Global Kalman filter VLBI and GPS analysis program. Release, 10*.
- Hill, K. C., Hall, R., Hillis, R. R., & Müller, R. D. (2003). *Mesozoic-Cenozoic evolution of Australia's New Guinea margin in a west Pacific context. Evolution and Dynamics of the Australian Plate*. (Vol. 372, p. 0). Geological Society of America.
- Hinschberger, F., Malod, J.-A., Dymont, J., Honthaas, C., Réhault, J.-P., & Burhanuddin, S. (2001). Magnetic lineations constraints for the back-arc opening of the late Neogene south Banda basin (eastern Indonesia). *Tectonophysics*, 333(1–2), 47–59. [https://doi.org/10.1016/S0040-1951\(00\)00266-3](https://doi.org/10.1016/S0040-1951(00)00266-3)
- Hinschberger, F., Malod, J.-A., Réhault, J.-P., Dymont, J., Honthaas, C., Villeneuve, M., & Burhanuddin, S. (2000). Origine et evolution du bassin Nord-Banda (Indonesie): Apport des donnees magnetiques. *Comptes Rendus de l'Academie des Sciences - Series IIA: Earth and Planetary Science*, 331(7), 507–514. [https://doi.org/10.1016/S1251-8050\(00\)01438-5](https://doi.org/10.1016/S1251-8050(00)01438-5)
- Irsyam, M., Cummins, P. R., Asrurifak, M., Faizal, L., Natawidjaja, D. H., Widiyantoro, S., et al. (2020). Development of the 2017 national seismic hazard maps of Indonesia. *Earthquake Spectra*, 36(1_suppl), 112–136. <https://doi.org/10.1177/8755293020951206>
- Jaya, A., & Nishikawa, O. (2013). Paleostress reconstruction from calcite twin and fault-slip data using the multiple inverse method in the East Walanae fault zone: Implications for the Neogene contraction in South Sulawesi, Indonesia. *Journal of Structural Geology*, 55, 34–49. <https://doi.org/10.1016/j.jsg.2013.07.006>
- Katili, J. A. (1986). *Geology and hydrocarbon potential of the Arafura Sea*. In M. T. Halbouty (Ed.), *Future Petroleum Province of the Worlds*.
- Kearey, P., Klepeis, K. A., & Vine, F. J. (2013). *Global tectonics*. John Wiley & Sons.
- Koulali, A., McClusky, S., Susilo, S., Leonard, Y., Cummins, P., Tregoning, P., et al. (2017). The kinematics of crustal deformation in Java from GPS observations: Implications for fault slip partitioning. *Earth and Planetary Science Letters*, 458, 69–79. <https://doi.org/10.1016/j.epsl.2016.10.039>
- Koulali, A., Susilo, S., McClusky, S., Meilano, I., Cummins, P., Tregoning, P., et al. (2016). Crustal strain partitioning and the associated earthquake hazard in the eastern Sunda-Banda Arc. *Geophysical Research Letters*, 43(5), 1943–1949. <https://doi.org/10.1002/2016gl067941>
- Koulali, A., Tregoning, P., McClusky, S., Stanaway, R., Wallace, L., & Lister, G. (2015). New Insights into the present-day kinematics of the central and Western Papua New Guinea from GPS. *Geophysical Journal International*, 202(2), 993–1004. <https://doi.org/10.1093/gji/ggv200>
- Kreemer, C., Blewitt, G., & Klein, E. C. (2014). A geodetic plate motion and global strain rate model. *Geochemistry, Geophysics, Geosystems*, 15(10), 3849–3889. <https://doi.org/10.1002/2014gc005407>
- Larson, K. M., Freymueller, J. T., & Philipson, S. (1997). Global plate velocities from the global positioning system. *Journal of Geophysical Research*, 102(B5), 9961–9981.
- Lindley, I. D. (2006). *Extensional and vertical tectonics in the new Guinea islands: Implications for island arc evolution*. In G. Lavecchia & G. (Eds.) (pp. 403–426).
- Lonsdale, P. (1978). Near-bottom reconnaissance of a fast-slipping transform fault zone at the Pacific-Nazca Plate Boundary. *The Journal of Geology*, 86(4), 451–472. <https://doi.org/10.1086/649712>
- McCaffrey, R. (1989). Seismological constraints and speculations on Banda Arc tectonics. *Netherlands Journal of Sea Research*, 24(2–3), 141–152. [https://doi.org/10.1016/0077-7579\(89\)90145-2](https://doi.org/10.1016/0077-7579(89)90145-2)
- McCaffrey, R. (2002). Irian Jaya 2002, the GAGE Facility operated by UNAVCO, Inc. Dataset. *GPS/GNSS Observations*. <https://doi.org/10.7283/T5765CDW>
- McCaffrey, R. (2005). Irian Jaya 2004, the GAGE Facility operated by UNAVCO, Inc. Dataset. *GPS/GNSS Observations*. <https://doi.org/10.7283/T5BZ643V>
- McCaffrey, R. (2009). Time-dependent inversion of three-component continuous GPS for steady and transient sources in northern Cascadia. *Geophysical Research Letters*, 36(7). <https://doi.org/10.1029/2008gl036784>
- McCaffrey, R., & Abers, G. A. (1991). Orography in arc-continent collision: The Banda arc and Western New Guinea. *Geology*, 19(6), 563–566. [https://doi.org/10.1130/0091-7613\(1991\)019<0563:oiact>2.3.co;2](https://doi.org/10.1130/0091-7613(1991)019<0563:oiact>2.3.co;2)
- McCaffrey, R., Long, M. D., Goldfinger, C., Zwick, P. C., Nabelek, J. L., Johnson, C. K., & Smith, C. (2000). Rotation and plate locking at the southern Cascadia subduction zone. *Geophysical Research Letters*, 27(19), 3117–3120. <https://doi.org/10.1029/2000gl011768>
- McCaffrey, R., & Nábělek, J. (1984). The geometry of back arc thrusting along the eastern Sunda arc, Indonesia: Constraints from earthquake and gravity data. *Journal of Geophysical Research*, 89(B7), 6171–6179. <https://doi.org/10.1029/jb089ib07p06171>
- McCaffrey, R., Stein, S., & Freymueller, J. (2002). Crustal block rotations and plate coupling. *Plate Boundary Zones, Geodyn. Ser.*, 30, 101–122.
- McKenzie, D. P., & Morgan, W. J. (1969). Evolution of triple junctions. *Nature*, 224(5215), 125–133. <https://doi.org/10.1038/224125a0>
- Meade, B. J., & Hager, B. H. (2005). Block models of crustal motion in southern California constrained by GPS measurements. *Journal of Geophysical Research*, 110(B3), B03403. <https://doi.org/10.1029/2004jb003209>
- Meilano, I., Salman, R., Rahmadani, S., Shi, Q., Susilo, S., Lindsey, E., et al. (2021). Source characteristics of the 2019 M w 6.5 Ambon, eastern Indonesia, earthquake inferred from seismic and geodetic data. *Seismological Society of America*, 92(6), 3339–3348. <https://doi.org/10.1785/0220210021>
- Memmo, V., Bertoni, C., Masini, M., Alvarez, J., Imran, Z., Echanove, A., & Orange, D. (2013). Deposition and deformation in the recent Biak Basin (Papua province, eastern Indonesia).
- Miller, M. S., Zhang, P., Dahlquist, M. P., West, A. J., Becker, T. W., & Harris, C. (2021). Inherited lithospheric structures control arc-continent collisional heterogeneity. *Geology*, 49(6), 652–656. <https://doi.org/10.1130/g48246.1>
- Nugroho, H., Harris, R., Lestariya, A. W., & Maruf, B. (2009). Plate boundary reorganization in the active Banda Arc–continent collision: Insights from new GPS measurements. *Tectonophysics*, 479(1–2), 52–65. <https://doi.org/10.1016/j.tecto.2009.01.026>
- Ott, B., & Mann, P. (2015). Late Miocene to Recent formation of the A ure-M oresby fold-thrust belt and foreland basin as a consequence of Woodlark microplate rotation, Papua New Guinea. *Geochemistry, Geophysics, Geosystems*, 16(6), 1988–2004. <https://doi.org/10.1002/2014gc005668>
- Phillips, D. A. (2003). Crustal motion studies in the Southwest Pacific: Geodetic measurements of plate convergence in Tonga, Vanuatu and the Solomon Islands.
- Pownall, J. M., Hall, R., & Lister, G. S. (2016). Rolling open Earth's deepest forearc basin. *Geology*, 44(11), 947–950. <https://doi.org/10.1130/g38051.1>
- Press, W. H., Flannery, B. P., Teukolsky, S. A., & Vetterling, W. T. (1989). *Numerical Recipes*. Cambridge university press Cambridge, UK.
- Pubellier, M., & Ego, F. (2002). Anatomy of an escape tectonic zone: Western Irian Jaya (Indonesia). *Tectonics*, 21(4), 1–1–1–16. <https://doi.org/10.1029/2001tc901038>
- Puntodewo, S., McCaffrey, R., Calais, E., Bock, Y., Rais, J., Subarya, C., et al. (1994). GPS measurements of crustal deformation within the Pacific-Australia plate boundary zone in Irian Jaya, Indonesia. *Tectonophysics*, 237(3–4), 141–153. [https://doi.org/10.1016/0040-1951\(94\)90251-8](https://doi.org/10.1016/0040-1951(94)90251-8)
- Rahmadani, S., Meilano, I., Susilo, S., Sarsito, D. A., Abidin, H. Z., & Supendi, P. (2022). Geodetic observation of strain accumulation in the Banda Arc region. *Geomatics, Natural Hazards and Risk*, 13(1), 2579–2596. <https://doi.org/10.1080/19475705.2022.2126799>

- Reilinger, R., McClusky, S., Vernant, P., Lawrence, S., Ergintav, S., Cakmak, R., et al. (2006). GPS constraints on continental deformation in the Africa-Arabia-Eurasia continental collision zone and implications for the dynamics of plate interactions. *Journal of Geophysical Research*, *111*(B5). <https://doi.org/10.1029/2005jb004051>
- Roosmawati, N., & Harris, R. (2009). Surface uplift history of the incipient Banda arc-continent collision: Geology and synorogenic foraminifera of Rote and Savu Islands, Indonesia. *Tectonophysics*, *479*(1–2), 95–110. <https://doi.org/10.1016/j.tecto.2009.04.009>
- Sapiie, B., Natawidjaya, D., & Cloos, M. (1999). Strike-slip tectonics of new Guinea: Transform motion between the Caroline and Australian plates. *Developments in Indonesian tectonics and structural geology: Proceedings of the Indonesian Association of Geologists*, *1*, 1–15.
- Savage, J., & Burford, R. (1973). Geodetic determination of relative plate motion in central California. *Journal of Geophysical Research*, *78*(5), 832–845. <https://doi.org/10.1029/jb078i005p00832>
- Silver, E. A., Abbott, L. D., Kirchoff-Stein, K. S., Reed, D. L., Bernstein-Taylor, B., & Hilyard, D. (1991). Collision propagation in Papua New Guinea and the Solomon Sea. *Tectonics*, *10*(5), 863–874. <https://doi.org/10.1029/91tc00867>
- Silver, E. A., Reed, D., McCaffrey, R., & Joyodiwiryo, Y. (1983). Back arc thrusting in the eastern Sunda arc, Indonesia: A consequence of arc-continent collision. *Journal of Geophysical Research*, *88*(B9), 7429–7448. <https://doi.org/10.1029/jb088ib09p07429>
- Simons, W., Socquet, A., Vigny, C., Ambrosius, B., Haji Abu, S., Promthong, C., et al. (2007). A decade of GPS in Southeast Asia: Resolving Sundaland motion and boundaries. *Journal of Geophysical Research*, *112*(B6), B06420. <https://doi.org/10.1029/2005jb003868>
- Socquet, A., Simons, W., Vigny, C., McCaffrey, R., Subarya, C., Sarsito, D., et al. (2006). Microblock rotations and fault coupling in SE Asia triple junction (Sulawesi, Indonesia) from GPS and earthquake slip vector data. *Journal of Geophysical Research*, *111*(B8), B08409. <https://doi.org/10.1029/2005jb003963>
- Spakman, W., & Hall, R. (2010). Surface deformation and slab–mantle interaction during Banda arc subduction rollback. *Nature Geoscience*, *3*(8), 562–566. <https://doi.org/10.1038/ngeo917>
- Spencer, C. J., Harris, R. A., & Major, J. R. (2016). Provenance of Permian–Triassic Gondwana Sequence units accreted to the Banda Arc in the Timor region: Constraints from zircon U–Pb and Hf isotopes. *Gondwana Research*, *38*, 28–39. <https://doi.org/10.1016/j.gr.2015.10.012>
- Stein, S., & Gordon, R. G. (1984). Statistical tests of additional plate boundaries from plate motion inversions. *Earth and Planetary Science Letters*, *69*(2), 401–412. [https://doi.org/10.1016/0012-821x\(84\)90198-5](https://doi.org/10.1016/0012-821x(84)90198-5)
- Stevens, C. W., McCaffrey, R., Bock, Y., Genrich, J. F., Pubellier, M., & Subarya, C. (2002). Evidence for block rotations and basal shear in the world's fastest slipping continental shear zone in NW New Guinea. *Plate Boundary Zones, Geodyn. Ser.*, *30*, 87–99.
- Supendi, P., Nugraha, A., Widiyantoro, S., Pesicek, J., Thurber, C., Abdullah, C., et al. (2020). Relocated aftershocks and background seismicity in eastern Indonesia shed light on the 2018 Lombok and Palu earthquake sequences. *Geophysical Journal International*, *221*(3), 1845–1855. <https://doi.org/10.1093/gji/ggaa118>
- Supendi, P., Rawlinson, N., Prayitno, B. S., Widiyantoro, S., Simanjuntak, A., Palgunadi, K. H., et al. (2022). The Kalaotoa Fault: A newly identified fault that generated the M w 7.3 Flores Sea earthquake. *The Seismic Record*, *2*(3), 176–185. <https://doi.org/10.1785/0320220015>
- Taylor, B. (1979). Bismarck Sea: Evolution of a back-arc basin. *Geology*, *7*(4), 171–174. [https://doi.org/10.1130/0091-7613\(1979\)7<171:bseoab>2.0.co;2](https://doi.org/10.1130/0091-7613(1979)7<171:bseoab>2.0.co;2)
- Taylor, B., Crook, K., Sinton, J., Petersen, L., Mallonee, R., Kellogg, J., & Martinez, F. (1991). Manus Basin, Papua New Guinea, SeaMARC II sidescan sonar imagery, bathymetry, magnetic anomalies, and free air gravity anomalies, Pacific Seafloor Atlas. *Pacific Seafloor Atlas, Sheet*, *7*.
- Tregoning, P. (2002). Plate kinematics in the Western Pacific derived from geodetic observations. *Journal of Geophysical Research*, *107*(B1), ECV 7-1-ECV 7-8. <https://doi.org/10.1029/2001jb000406>
- Tregoning, P., Brunner, F., Bock, Y., Puntodewo, S., McCaffrey, R., Genrich, J., et al. (1994). First geodetic measurement of convergence across the Java Trench. *Geophysical Research Letters*, *21*(19), 2135–2138. <https://doi.org/10.1029/94gl01856>
- Tregoning, P., Burgette, R., McClusky, S., Lejeune, S., Watson, C. S., & McQueen, H. (2013). A decade of horizontal deformation from great earthquakes. *Journal of Geophysical Research: Solid Earth*, *118*(5), 2371–2381. <https://doi.org/10.1002/jgrb.50154>
- Tregoning, P., Jackson, R. J., McQueen, H., Lambeck, K., Stevens, C., Little, R. P., et al. (1999). Motion of the South Bismarck plate, Papua New Guinea. *Geophysical Research Letters*, *26*(23), 3517–3520. <https://doi.org/10.1029/1999gl010840>
- Tregoning, P., Lambeck, K., Stolz, A., Morgan, P., McClusky, S. C., Beek, P., et al. (1998). Estimation of current plate motions in Papua New Guinea from Global Positioning System observations. *Journal of Geophysical Research*, *103*(B6), 12181–12203.
- Tregoning, P., & McQueen, H. (2001). Resolving slip vector azimuths and plate motion along the southern boundary of the South Bismarck Plate, Papua New Guinea. *Australian Journal of Earth Sciences*, *48*(5), 745–750. <https://doi.org/10.1046/j.1440-0952.2001.00896.x>
- Tregoning, P., McQueen, H., Lambeck, K., Jackson, R., Little, R., Saunders, S., & Rosa, R. (2000). Present-day crustal motion in Papua New Guinea. *Earth Planets and Space*, *52*(10), 727–730. <https://doi.org/10.1186/bf03352272>
- Tregoning, P., Tan, F., Gilliland, J., McQueen, H., & Lambeck, K. (1998b). Present-day crustal motion in the Solomon Islands from GPS observations. *Geophysical Research Letters*, *25*(19), 3627–3630. <https://doi.org/10.1029/98gl52761>
- Wallace, L. M., Ellis, S., Little, T., Tregoning, P., Palmer, N., Rosa, R., et al. (2014). Continental breakup and UHP rock exhumation in action: GPS results from the Woodlark Rift, Papua New Guinea. *Geochemistry, Geophysics, Geosystems*, *15*(11), 4267–4290. <https://doi.org/10.1002/2014gc005458>
- Wallace, L. M., Stevens, C., Silver, E., McCaffrey, R., Loratung, W., Hasiata, S., et al. (2004). GPS and seismological constraints on active tectonics and arc-continent collision in Papua New Guinea: Implications for mechanics of microplate rotations in a plate boundary zone. *Journal of Geophysical Research*, *109*(B5). <https://doi.org/10.1029/2003jb002481>
- Wang, K., Wells, R., Mazzotti, S., Hyndman, R. D., & Sagiya, T. (2003). A revised dislocation model of interseismic deformation of the Cascadia subduction zone. *Journal of Geophysical Research*, *108*(B1). <https://doi.org/10.1029/2001jb001227>
- Watkinson, I. M., & Hall, R. (2017). Fault systems of the eastern Indonesian triple junction: Evaluation of Quaternary activity and implications for seismic hazards. *Geological Society, London, Special Publications*, *441*(1), 71–120. <https://doi.org/10.1144/sp441.8>
- Weissel, J. K., Taylor, B., & Karner, G. D. (1982). The opening of the Woodlark Basin, subduction of the Woodlark spreading system, and the evolution of northern Melanesia since mid-Pliocene time. *Tectonophysics*, *87*(1–4), 253–277. [https://doi.org/10.1016/0040-1951\(82\)90229-3](https://doi.org/10.1016/0040-1951(82)90229-3)
- Williams, P., Pigram, C., Dow, D., & Amiruddin (1984). Melange production and the importance of shale diapirism in accretionary terrains. *Nature*, *309*(5964), 145–146. <https://doi.org/10.1038/309145a0>
- Willmott, C. J., & Matsuura, K. (2006). On the use of dimensioned measures of error to evaluate the performance of spatial interpolators. *International Journal of Geographical Information Science*, *20*(1), 89–102. <https://doi.org/10.1080/13658810500286976>

References From the Supporting Information

- Argus, D. F., & Gordon, R. G. (1991). No-net-rotation model of current plate velocities incorporating plate motion model NUVEL-1. *Geophysical Research Letters*, *18*(11), 2039–2042. <https://doi.org/10.1029/91gl01532>
- Beavan, J., Tregoning, P., Bevis, M., Kato, T., & Meertens, C. (2002). Motion and rigidity of the Pacific Plate and implications for plate boundary deformation. *Journal of Geophysical Research*, *107*(B10), 19–15.